Contrasting Daytime and Nighttime Precipitation Variability between Observations and Eight Reanalysis Products from 1979 to 2014 in China

CHUNLÜE ZHOU AND KAICUN WANG

College of Global Change and Earth System Science, Beijing Normal University, Beijing, China

(Manuscript received 28 September 2016, in final form 25 April 2017)

ABSTRACT

Daytime (0800–2000 Beijing time) and nighttime (2000–0800 Beijing time) precipitation at approximately 2100 stations in China from 1979 to 2014 was used to evaluate eight current reanalyses. Daytime, nighttime, and nighttime–daytime contrast of precipitation were examined in aspects of climatology, seasonal cycle, interannual variability, and trends. The results show that the ECMWF interim reanalysis (ERA-Interim), ERA-Interim/Land, Japanese 55-year Reanalysis (JRA-55), and NCEP Climate Forecast System Reanalysis (CFSR) can reproduce the observed spatial pattern of nighttime–daytime contrast in precipitation amount, exhibiting a positive center over the eastern Tibetan Plateau and a negative center over southeastern China. All of the reanalyses roughly reproduce seasonal variations of nighttime and daytime precipitation, but not always nighttime–daytime contrast. The reanalyses overestimate drizzle and light precipitation frequencies by greater than 31.5% and underestimate heavy precipitation frequencies by less than −30.8%. The reanalyses successfully reproduce interannual synchronizations of daytime and nighttime precipitation frequencies and amounts with an averaged correlation coefficient r of 0.66 against the observed data but overestimate their year-to-year amplitudes by approximately 64%. The trends in nighttime, daytime, and nighttime–daytime contrast of the observed precipitation amounts are mainly dominated by their frequencies ($r = 0.85$). Less than moderate precipitation frequency has exhibited a significant downward trend (−2.5% decade^{-1} during nighttime and −1.7% decade^{-1} during daytime) since 1979, which is roughly captured by the reanalyses. However, only JRA-55 captures the observed trend of nighttime precipitation intensity (2.4% decade^{-1}), while the remaining reanalyses show negative trends. Overall, JRA-55 and CFSR provide the best reproductions of the observed nighttime–daytime contrast in precipitation intensity, although they have considerable room for improvement.

1. Introduction

The diurnal variation of precipitation is an important aspect of Earth's weather and climate and is often related to thermodynamic and dynamic processes of water and energy fluxes, which greatly arouse the interest of scientists. Therefore, a lot of studies have been conducted to investigate the timing of diurnal precipitation peaks through the use of precipitation observation worldwide.

Summer precipitation tends to be more frequent in the afternoon over inland regions and from night to early morning over coastal zones and most oceans, as revealed by previous studies in different regions, including Japan (Oki and Musiake 1994), China (Yu et al. 2007b; Zhou et al. 2008; Yu et al. 2010; Zhuo et al. 2014), India (Deshpande and Goswami 2014), western Africa (Pinker et al. 2006), the tropical Americas (Poveda et al. 2005), and the tropics and subtropics (Nesbitt and Zipser 2003). Specifically, summer precipitation peaks at approximately midnight over the Tibetan Plateau and its eastern periphery (Yu et al. 2007b), although it exhibits a late-evening peak and a secondary morning precipitation peak in the valleys and large lakes of the Tibetan Plateau (Chow and Chan 2009; Liu et al. 2009;

Denotes content that is immediately available upon publication as open access.

Supplemental information related to this paper is available at the Journals Online website: http://dx.doi.org/10.1175/JCLI-D-16-0702.s1.

Corresponding author: Kaicun Wang, kcwang@bnu.edu.cn

DOI: 10.1175/JCLI-D-16-0702.1

Singh and Nakamura 2009). Yu et al. (2007a) reported that long-duration stratiform precipitation tends to occur in the early morning, whereas short-duration convective precipitation usually occurs in the late afternoon during warm seasons over central eastern China.

Over the southeastern and western United States, summer precipitation often occurs in the late afternoon, although it frequently occurs from midnight to the early morning in the regions east of the Rockies and Great Plains. The weak precipitation peaks in the other seasons usually occur in the morning over most of the United States (Wallace 1975; Dai and Deser 1999; Dai et al. 1999; Dai 2001b). Additionally, the precipitation frequency has a much larger diurnal variation than the precipitation intensity (Dai 2001b).

Therefore, precipitation can be divided into two distinct types based on its timing: afternoon convective precipitation and nocturnal cooling precipitation (Wallace 1975; Dai et al. 1999; Dai 2001b; Yu et al. 2007b; Zhou et al. 2008; Yu et al. 2010; Houze 2012). Numerous physical mechanisms have been introduced to explain the two types of precipitation. In general terms, they can be summarized as "a local moist/thermodynamical response."

As the sun rises, the surface is heated by solar radiation and reaches its maximum temperature at noon. The atmosphere continues to be heated and then reaches its maximum temperature in early afternoon. Synchronically, atmospheric pressure, wind, and atmospheric water content, etc., exhibit very regular diurnal variations that result in the diurnal cycle of precipitation (Wallace 1975; Dai et al. 1999; Dai and Wang 1999; Dai 2001a). Therefore, afternoon convective precipitation is generally caused by low-level atmospheric instability and moist convergence caused by solar heating (Wallace 1975; Dai et al. 1999). Nocturnal cooling precipitation is mainly generated by the substantial moisture condensation caused by nocturnal radiative cooling at the cloud top (Randall et al. 1991; Xu and Randall 1995; Lin et al. 2000) and the resultant high relative humidity for precipitation at night (Sui et al. 1997).

Additionally, orographically induced circulation (Liu et al. 2009; Houze 2012) and land–sea breeze circulations (Wallace 1975; Silva Dias et al. 1987; Dai and Deser 1999) are also responsible for diurnal precipitation variation via mechanical and thermal forcings. Besides, boundary layer growth, evolution of thermodynamic and dynamic processes (e.g., the lifting condensation level and turbulent kinetic energy), moistening of the lower midtroposphere, and convection triggers also play a role (Dai 2001a,b; Sun et al. 2006; Schneider et al. 2010).

Because of the purely model-derived precipitation in the reanalysis products, it is important to examine whether their models can reproduce diurnal variation of the observed precipitation. However, existing evaluations of precipitation modeled by reanalysis products have mostly concentrated on time scales longer than 24 h, which would miss the diurnally driven processes and relevant information. Existing reanalysis products, including the Interim ECMWF interim reanalysis (ERA-Interim), the 40-yr ECMWF Re-Analysis (ERA-40), National Centers for Environmental Prediction (NCEP)–National Center for Atmospheric Research (NCAR) reanalysis (NCEP R1), NCEP–U.S. Department of Energy (DOE) AMIP-II reanalysis (NCEP R2), Modern-Era Retrospective Analysis for Research and Applications (MERRA), and the Japanese 25-year Reanalysis Project (JRA-25) products, have been reported to reasonably reproduce the climatology and interannual variability of precipitation over the Tibetan Plateau (Wang and Zeng 2012), East Asia (Huang et al. 2016), South America (Betts and Jakob 2002), and the global monsoon zones (Bosilovich et al. 2008; Lin et al. 2014).

Huang et al. (2016) suggested that 0–0.5 mm day^{-1} precipitation frequencies were overestimated in all of the products, and >14.8 mm day^{-1} precipitation frequencies over East Asia were overestimated by NCEP R2 and JRA-25; in addition, de Leeuw et al. (2015) reported that >15 mm day^{-1} precipitation frequencies over England and Wales were underestimated by ERA-Interim. Lin et al. (2014) indicated the global monsoon precipitation tendency (except for North African monsoon precipitation) can be reasonably reproduced by most reanalysis products. Ashouri et al. (2016) reported that MERRA produces a spurious trend of the 99th percentile precipitation in the central United States. You et al. (2015) argued that large discrepancies in precipitation trends occur over the Tibetan Plateau among most reanalysis products because of different assimilation systems. However, there is no study addressing whether the reanalyses can accurately reproduce the partitioning of daily precipitation into nighttime and daytime precipitation.

Few studies have been conducted to investigate the performance of diurnal precipitation variation in the reanalysis models. Betts and Jakob (2002) analyzed the mean diurnal cycle of precipitation from ECMWF model over South America and suggested that the ECMWF model cannot describe well the morning growth of the nonprecipitating convective boundary layer. Chen et al. (2014) reported that the Japanese 55-year Reanalysis (JRA-55) product could represent an increasing percentage of morning precipitation from 1966 to 2005 over the eastern plains of China that was revealed by Yuan et al. (2013). Dai (2006) found that the precipitation frequency at reduced intensities was too

high in the global coupled climate models. Therefore, additional efforts should be made to systematically evaluate diurnal precipitation variation in multiple reanalysis products (from old to new generations) and over larger regions, with focus on the partitioning of daily precipitation into nighttime and daytime precipitation, to provide insights into the various precipitation-related parameterizations.

Furthermore, because of the anthropogenic greenhouse effect, an asymmetric diurnal warming occurs (e.g., minimum air temperature during nighttime generally warms faster than maximum air temperature during daytime) (IPCC 2013; Zhou and Wang 2016b,a); therefore, the very regular diurnal variation of temperature is substantially modified. Moreover, the East Asian summer–winter monsoon has been weakening since the 1980s (Wang 2001; Wang et al. 2009). Therefore, whether diurnal precipitation variation presents a long-term trend and an asymmetric effect requires further investigation.

Because of the model-selected different parameterizations of precipitation processes, it is helpful to examine diurnal precipitation variation in reanalysis products. Here, the latest daytime [0800–2000 Beijing time (BT)] and nighttime (2000–0800 BT) precipitation dataset collected at approximately 2100 meteorological stations in China from 1979 to 2014 was used to comprehensively evaluate the modeling ability of nighttime, daytime precipitation, and their partitioning of eight old- and new-generation reanalysis products (i.e., from NCEP, ECMWF, MERRA, and JRA-55) via a multilevel (including the frequency, intensity, and amount of precipitation among the different categories from drizzle to heavy precipitation) and multiscale analysis (including climatology, seasonal cycle, interannual variability, and long-term trends). Our results show orographically induced circulations have an important impact on nighttime–daytime precipitation contrast over the Tibetan Plateau. The reanalysis products present the observed negative trends in nighttime and daytime precipitation frequencies and amounts but cannot reproduce their trends for nighttime–daytime contrasts. Only JRA-55 presents the observed positive trends in nighttime–daytime contrast of precipitation intensity, while the other seven reanalyses simulate an opposite trend.

2. Data and methods

a. *In situ observed precipitation dataset*

The accumulated precipitation observations were manually recorded by bucket rain gauges twice daily (i.e., 0800 and 2000 BT). The latest daytime (0800–2000 BT) and nighttime (2000–0800 BT) precipitation dataset collected at approximately 2400 meteorological stations in China from 1979 to 2014 was obtained from the China Meteorological Administration (CMA; http://data.cma.cn/en/?r=data/). This dataset has undergone a series of quality control measures and homogenization including outlier identification, internal consistency checks and spatial and temporal consistency checks (Ren et al. 2010). Moreover, the standard normalized homogeneity test (SNHT) method (Alexandersson 1986) was adopted to detect the homogeneity of precipitation time series and 35 out of about 2400 stations were found to show inhomogeneity (Shen and Xiong 2016). After these procedures and then manual review, 0.81% of data were checked and discarded.

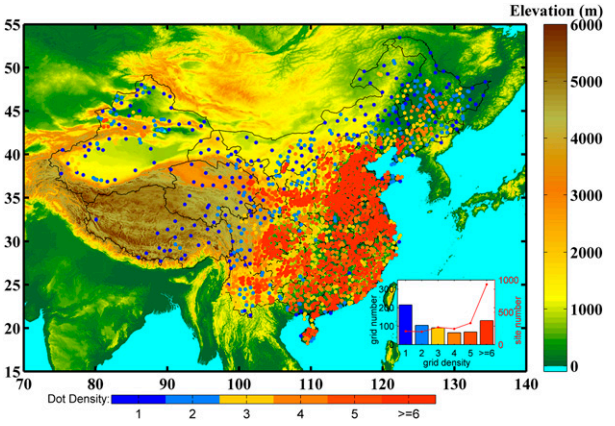

FIG. 1. Geographic distribution of approximately 2100 meteorological observation stations (colored dots) on the underlying topography (m) from the Global 30-arc-s elevation dataset (GTOPO30). The horizontal color bar denotes the number of stations falling in the 1° × 1° grid cell. The bottom-right inset panel presents the distribution of grid number and station number with grid density. The national average density of stations in the 1° × 1° grid cell over China is approximately 3.4 (5.3 over eastern China).

To reduce the impacts of record sampling and length, no less than 99% of the station records should have a subdaily time scale length for the period 1979–2014. Approximately 2100 stations met these requirements and were used in this study (Fig. 1). The stations are almost uniformly distributed across China, although they are sparsely distributed in the western Tibetan Plateau.

b. *Reanalyzed precipitation datasets*

Reanalysis datasets have been widely used in climate studies as important auxiliary observations (Dee et al. 2014). The performance of current reanalysis products, including old-generation products [i.e., NCEP R1 (Kalnay et al. 1996) and NCEP R2 (Kanamitsu et al. 2002)] and new-generation products [i.e., ERA-Interim

TABLE 1. Summary of the eight global reanalysis products examined in this study. Horizontal model resolutions designated with a T prefixed to a number mean a spectral model with triangular truncation at the given wavenumber.

Name	Organization	Model resolution	Downloaded grid	Time period	Assimilation system
NCEP R1	NOAA/NCEP and NCAR	T62 (~210 km)	192 × 94 Gaussian grid	1948 onward	3D-VAR
NCEP R2	NOAA/NCEP and DOE	T62 (~210 km)	192 × 94 Gaussian grid	1979 onward	3D-VAR
CFSR	NOAA/NCEP	T382 (~38 km)	1/2° × 1/2°	1979 onward	3D-VAR
MERRA	NASA GSFC GMAO	1/2° × 2/3° (~55 km)	1/2° × 2/3°	1979 onward	3D-VAR
MERRA land	NASA GSFC GMAO	1/2° × 2/3° (~55 km)	1/2° × 2/3°	1980 onward	4D-VAR
ERA-Interim	ECMWF	T255 (~80 km)	1° × 1°	1979 onward	4D-VAR
ERA-Interim/Land	ECMWF	T255 (~80 km)	1° × 1°	1979–2010	4D-VAR
JRA-55	JMA	T319 (~55 km)	5/4° × 5/4°	1958 onward	4D-VAR

(ERA-I; Dee et al. 2011), ERA-Interim/Land (ERA-I land; Balsamo et al. 2015), JRA-55 (Kobayashi et al. 2015), MERRA (Rienecker et al. 2011), MERRA land (Reichle et al. 2011), and NCEP Climate Forecast System Reanalysis (CFSR) (Saha et al. 2010)] in simulating diurnal precipitation variation at different model resolutions were evaluated in this study. MERRA, NCEP R1, NCEP R2, and CFSR adopt three-dimensional variational data assimilation systems (3D-VAR), whereas ERA-Interim, ERA-Interim/Land, JRA-55, and MERRA land employ four-dimensional variational data systems (4D-VAR) (Table 1). The reanalysis products assimilate many of the basic surface and upper-atmospheric fields, including the surface pressure, near-surface relative humidity, radiosonde-based specific humidity, wind fields, satellite-derived radiance, etc., from multiple sources. The MERRA land, which is a supplemental land surface data product of MERRA, includes a key change in precipitation forcing via the merging of unified gauge-based (Chen et al. 2008) and MERRA-derived precipitation since 1980, and it is considered to be more accurate for land surface hydrological studies (Reichle et al. 2011). However, both land products rely on their model simulations to partition precipitation into daytime and nighttime.

To assess the multiscale performance of the reanalysis products for precipitation, the nighttime (1200–2400 UTC, i.e., 2000–0800 BT) and daytime (0000–1200 UTC, i.e., 0800–2000 BT) precipitation were summed from the 6-hourly accumulated precipitation starting at the reference times (0000, 0600, 1200, and 1800 UTC) in the eight reanalysis datasets.

c. *Precipitation classification and trend calculation*

The average distance between each gauge and its nearest neighbor is 32.75 km over China (20.23 km over eastern China) and an average of approximately 3.4 stations (~5.3 stations over eastern China) fall in the 1° × 1° grid cell (Fig. 1) that makes the gridded error become small [illustrated by Figs. 5 and 6 in Miao et al. (2015)].

For spatiotemporal consistency, all of the reanalyzed precipitation data were resampled to 1° × 1° grids via the nearest area-weighted method [i.e., a linear interpolation functions on two-dimensional grids (Zhou and Wang 2016c)] and then matched to the available grids of the rain gauge observations (as shown Fig. 2). Because of low spatial correlation of precipitation (Xie et al. 2007; Shen and Xiong 2016), the grids in which no gauge station is located will not be included, which avoids the impact of any interpolations in grids without gauge stations (e.g., over the western Tibetan Plateau) on the evaluation results below.

In this study, a precipitation event was defined as precipitation P of no less than 0.1 mm $(12\,\mathrm{h})^{-1}$ (rain gauge precision) during nighttime or daytime. The precipitation event was categorized into four intensity categories: drizzle [$0.1 \le P < 1\,\mathrm{mm}\ (12\,\mathrm{h})^{-1}$] and light [$1 \le P < 10\,\mathrm{mm}\ (12\,\mathrm{h})^{-1}$], moderate [$10 \le P < 25\,\mathrm{mm}\ (12\,\mathrm{h})^{-1}$], and heavy precipitation [$P \ge 25\,\mathrm{mm}\ (12\,\mathrm{h})^{-1}$]. These classification criteria were used in many global analyses of precipitation (Dai 2006; Ma et al. 2015; Huang et al. 2016). Dai (2006) reported coupled climate models tend to precipitate too frequently at drizzle; therefore, it is necessary to separately discuss the seasonal cycles of daytime and nighttime drizzle.

Precipitation frequency was calculated as the number of days with precipitation in a category. The precipitation intensity for each category was calculated as the mean precipitation rates averaged among the precipitation events within the category. The precipitation amount in each category was the accumulated precipitation amount over the precipitation events within the category.

The trends in precipitation frequency, intensity, and amount were calculated based on

$$y = s\,t + b + \varepsilon, \tag{1}$$

where y refers to the precipitation characteristics, including the precipitation frequency, intensity, and

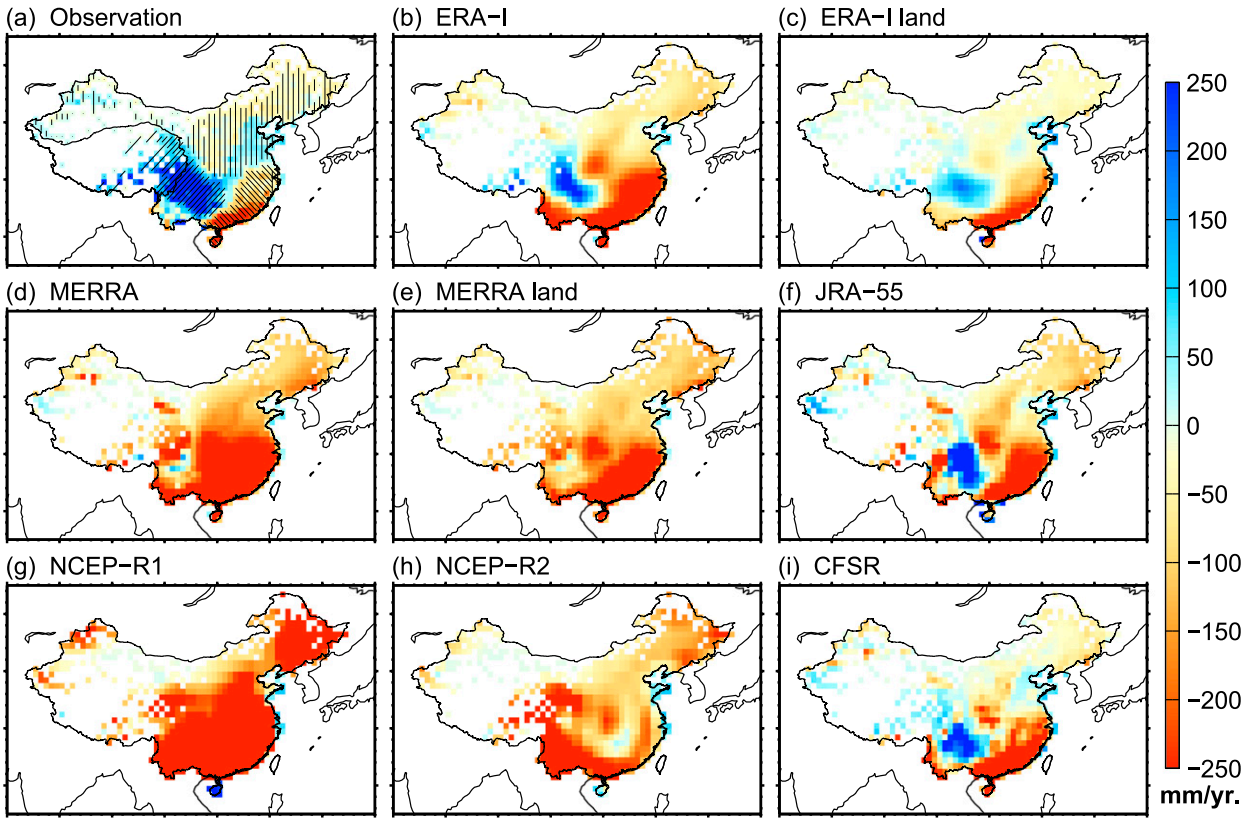

FIG. 2. Multiyear averages of nighttime–daytime contrasts in precipitation amounts (nighttime minus daytime; mm yr^{-1}) from (a) observations and the eight reanalysis products: (b) ERA-Interim, (c) ERA-Interim/Land, (d) MERRA, (e) MERRA land, (f) JRA-55, (g) NCEP R1, (h) NCEP R2, and (i) CFSR. A dipole pattern occurs over the Tibetan Plateau and its eastern periphery and southeastern China; therefore, the whole of China is divided into three regions in (a): the Tibetan Plateau and its eastern periphery (left diagonal hatching), southeastern China (right diagonal hatching), and northern China (vertical hatching).

amount; t refers to time; s refers to the corresponding trend; b refers to the interpolation; and ε refers to the error of the equation. Pearson's correlation and the two-tailed Student's t test were applied to calculate the correlation coefficients and trend significance.

3. Results

a. Climatological patterns in subdaily precipitation

Figure 2 shows the multiyear averages of nighttime–daytime contrasts in precipitation amounts from the observations and eight reanalysis datasets for the period 1979–2014. The observation exhibits an evident dipole field (approximately 495 mm yr^{-1}) that a positive center over the Tibetan Plateau and its eastern periphery (approximately 292 mm yr^{-1} averaged for the 31°–35°N, 100°–110°E land grids, which accounts for 21% of the daily precipitation accumulation) and a negative center over southeastern China (approximately −203 mm yr^{-1} averaged for the 21°–25°N, 110°–120°E land grids, which accounts for −19% of the daily precipitation accumulation) (Fig. 2a).

Based on the dipole pattern of nighttime–daytime precipitation contrast, the whole of China was divided into three subregions: the Tibetan Plateau and its eastern periphery, southeastern China, and northern China. Thus, the area-weighted average of precipitation characteristics over the three subregions could substantially reduce the impact of the gridded error on the evaluation results below. This method was widely applied to the evaluation of precipitation products [e.g., satellite-based precipitation products from the Global Precipitation Climatology Project (GPCP) (Huffman et al. 1997; Yin et al. 2004), Precipitation Estimation from Remotely Sensed Information Using Artificial Neural Networks–Climate Data Record (PERSIANN-CDR) (Ashouri et al. 2015), Climate Prediction Center (CPC) Morphing Technique (CMORPH) (Habib et al. 2012), and TRMM Multisatellite Precipitation Analysis (TMPA) products (Huffman et al. 2007)] and precipitation modeling (Dai 2006).

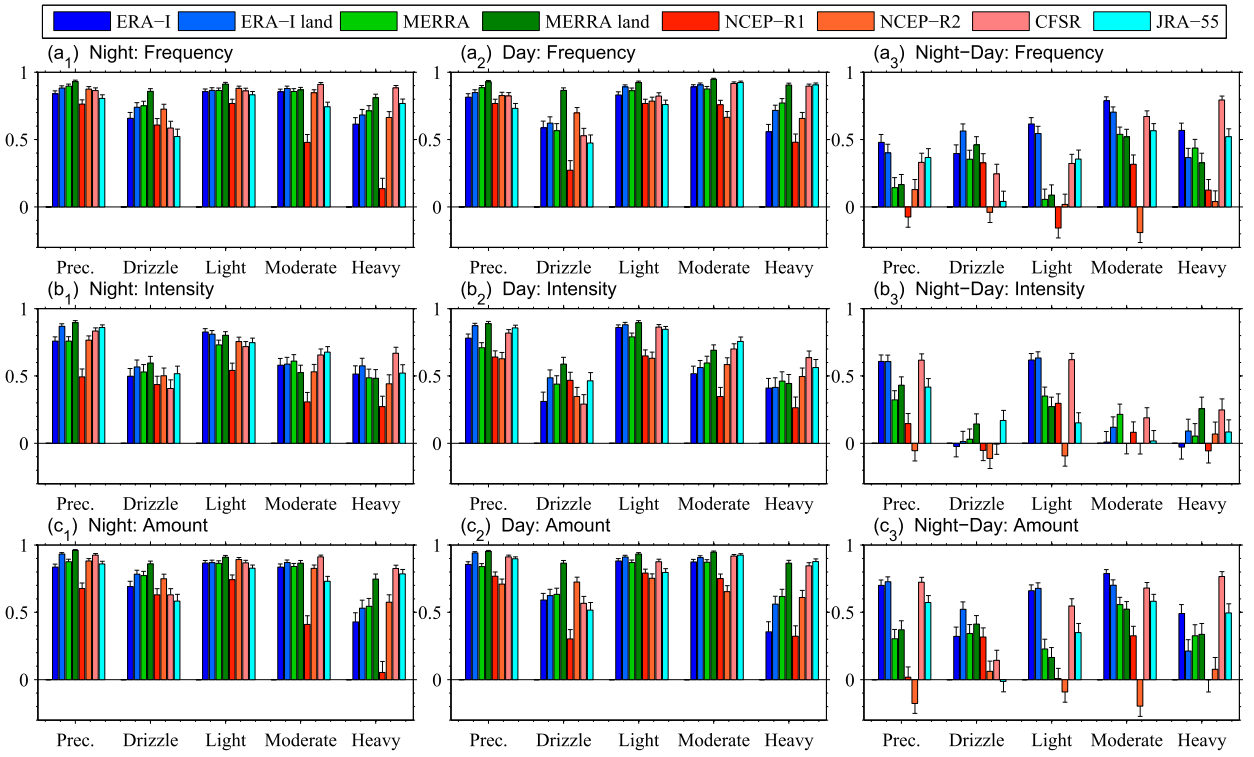

FIG. 3. Spatial correlation coefficients of multiyear average patterns from (left) nighttime, (center) daytime, and (right) nighttime–daytime contrasts of (a) precipitation frequencies, (b) intensities, and (c) amounts between the observed and reanalyzed precipitation datasets. The error bar denotes the 95% confidence intervals. The reanalysis datasets roughly reproduce nighttime and daytime precipitation patterns, but they show difficulties in precipitation partitioning between nighttime and daytime.

The ERA-Interim, ERA-Interim/Land, JRA-55, and CFSR products (with spatial resolution of <80 km; Table 1) roughly capture the dipole pattern (average of 469 mm yr^{-1} and spatial correlation of 0.68), although they underestimate the positive (average of 174 mm yr^{-1}) and negative centers (average of 148 mm yr^{-1}). On the contrary, the MERRA, MERRA land, NCEP R1, and NCEP R2 products cannot capture the dipole pattern (spatial correlation of 0.13) (Figs. 2b–i and Fig. 3c, right).

Over northern China, the observed nighttime–daytime precipitation contrast is near zero (approximately −3.04 mm yr^{-1}; Fig. 2a), mainly due to the two comparable peaks with long-duration precipitation in the early morning and short-duration precipitation in the late afternoon (Yu et al. 2007a,b). However, all of the reanalyses underestimate the nighttime–daytime precipitation contrast over northern China (Figs. 2b–i). Slightly negative nighttime–daytime precipitation contrast over the north China plain stretching from the eastern periphery of the Tibetan Plateau is observed (Fig. 2a), mainly owing to the northeastward propagation of long-term precipitation events in the early morning (Yu et al. 2007a,b).

Chen et al. (2009) and Chen et al. (2012) reported that there is a prevailing nocturnal precipitation peak at relatively lower locations (described by in situ observation often located in valleys) and afternoon precipitation peak at high locations (described by TRMM) over the Tibetan Plateau. Therefore, the nighttime–daytime precipitation contrast over the Tibetan Plateau might be as a result of the complexly orographically induced circulations. The exhibition of the dipole pattern in nighttime–daytime precipitation contrast between the Tibetan Plateau and southeastern China by reanalysis models can reflect skillful parameterizations of topography-related treatments and large-scale breeze circulation (Dai 2006; Chen et al. 2014).

Figure 3 shows that the spatial patterns of the nighttime and daytime precipitation frequencies, intensities, and amounts can be well represented by the eight reanalysis datasets and present multireanalysis-averaged correlation coefficients of 0.84, 0.78, and 0.86, respectively [standard deviation (SD) = 0.06, 0.11, and 0.08, respectively], although various performances in the different precipitation categories are observed for the reanalysis products (Figs. 3a–c, left and center). These spatial correlation coefficients of the eight reanalysis

datasets were calculated against the multiyear average observations in $1° \times 1°$ grids (Figs. 3a–c, left and center).

In view of precipitation partitioning between nighttime and daytime, ERA-Interim, ERA-Interim/Land, JRA-55, and CFSR are able to reproduce the spatial patterns of nighttime–daytime contrasts in precipitation frequencies and amounts among the different precipitation categories to a certain extent (multireanalysis average $r = 0.48$, SD = 0.19 and $r = 0.53$, SD = 0.21, respectively) (Figs. 3a,c, right, and Fig. S1 in the supplemental material). However, MERRA, MERRA land, NCEP R1, and NCEP R2 do not exhibit these capabilities (multireanalysis average $r = 0.18$, SD = 0.22 and $r = 0.20$, SD = 0.22, respectively) (Figs. 3a,c, right, and Fig. S1). Besides, MERRA land does not perform better in diurnal precipitation partitioning (Figs. 3a–c, right), likely because only monthly total precipitation observations are merged into the offline land surface model, and its diurnal cycle of precipitation is purely model simulation (Reichle et al. 2011; Balsamo et al. 2015). Additionally, ERA-Interim, ERA-Interim/Land, JRA-55, and CFSR roughly capture the spatial patterns of nighttime–daytime contrasts in the total and light precipitation intensities, although they cannot accurately capture those of the drizzle, moderate, and heavy categories (Fig. 3b, right, and Fig. S2 in the supplemental material).

b. *Seasonal cycles of subdaily precipitation*

Figure 4 shows that the eight reanalysis datasets can represent the seasonal shape of the nighttime and daytime precipitation frequencies over China except for the daytime drizzle frequencies (Figs. 4a,b). For daytime drizzle, ERA-Interim, ERA-Interim/Land, MERRA, and MERRA land roughly reproduce the seasonal shape over northern China (Fig. 5a, right), whereas NCEP R1, NCEP R2, and CFSR exhibit opposite shapes over China and its three subregions (Figs. 4b, left center, and 5a), which is mainly because these products overestimate moderate precipitation frequencies by 220%, 105%, and 58% during summer daytime, respectively (Fig. 4b, right center). These overestimations are likely caused by frequent firing of moist convection in the models (Dai 2006).

The total precipitation frequencies are overestimated by 31.5%–88.7% during nighttime and 42.7%–111.8% during daytime (Figs. 4a,b, left). Specifically, drizzle and light precipitation frequencies are overestimated by 37.2%–101.3% during nighttime and 41.4%–127.4% during daytime (Figs. 4a,b, left center and center). Heavy precipitation frequencies are underestimated from −30.8% to −88.7% during nighttime and from −43.9% to −88.1% during daytime (Figs. 4a,b, right). The overestimations of drizzle to light precipitation frequencies and underestimations of heavy precipitation frequencies indicate that the initiation of moist convection is relatively easy (Dai 2001b; Trenberth et al. 2003), which decreases the frequency of deep convective precipitation. This inaccurate parameterization of moist convection further results in an increased frequency of shallow convective precipitation, as indicated by the large overestimation of moderate precipitation frequencies during summer daytime (Fig. 4b, right center).

These results discover an important detail that the precipitation frequency overestimation of $>14.8\,\mathrm{mm\,day^{-1}}$ over East Asia by NCEP R2 (Huang et al. 2016) is mainly caused by the overestimated shallow convective precipitation during daytime (Fig. 4b, right center). ERA-Interim and ERA-Interim/Land underestimate moderate precipitation frequencies during nighttime and daytime (Figs. 4a,b, right center), which is consistent with the underestimated results of the ERA-Interim product over England and Wales (de Leeuw et al. 2015).

The observed nighttime–daytime contrast of precipitation frequency exhibits an obvious seasonal cycle that is well captured by JRA-55 (followed by ERA-Interim/Land, NCEP R2, and CFSR) but largely overestimated by MERRA, MERRA land, ERA-Interim, and NCEP R1 (Fig. 4c, left). This result indicates that JRA-55 (followed by ERA-Interim/Land, NCEP R2, and CFSR) may accurately describe the partitioning of precipitation frequencies despite presenting significant overestimations of the nighttime and daytime precipitation frequencies.

However, the eight reanalysis products fail to represent the seasonal cycles of the nighttime–daytime contrasts of drizzle frequencies, mainly resulting from model deficiencies in daytime drizzle frequencies (Figs. 4b,c, left center). The seasonal amplitudes of nighttime–daytime contrasts in light and moderate precipitation frequencies are exaggerated by the reanalysis products (Fig. 4c, center and right center). The nighttime–daytime contrast of heavy precipitation frequency over China exhibits a summer maximum cycle in the observation (Fig. 4c, right), primarily caused by that over the Tibetan Plateau and its eastern periphery (Figs. 2a and 5c, right, and Fig. S3a in the supplemental material). However, most of the reanalysis products (except for CFSR and ERA-Interim/Land) incorrectly depict this cycle (Fig. 4c, right, and Figs. S3c,i in the supplemental material).

The nighttime and daytime precipitation intensities (except for the drizzle category) in most reanalysis products (except for NCEP R1 and NCEP R2) are underestimated (Figs. 6a,b). The overestimation of

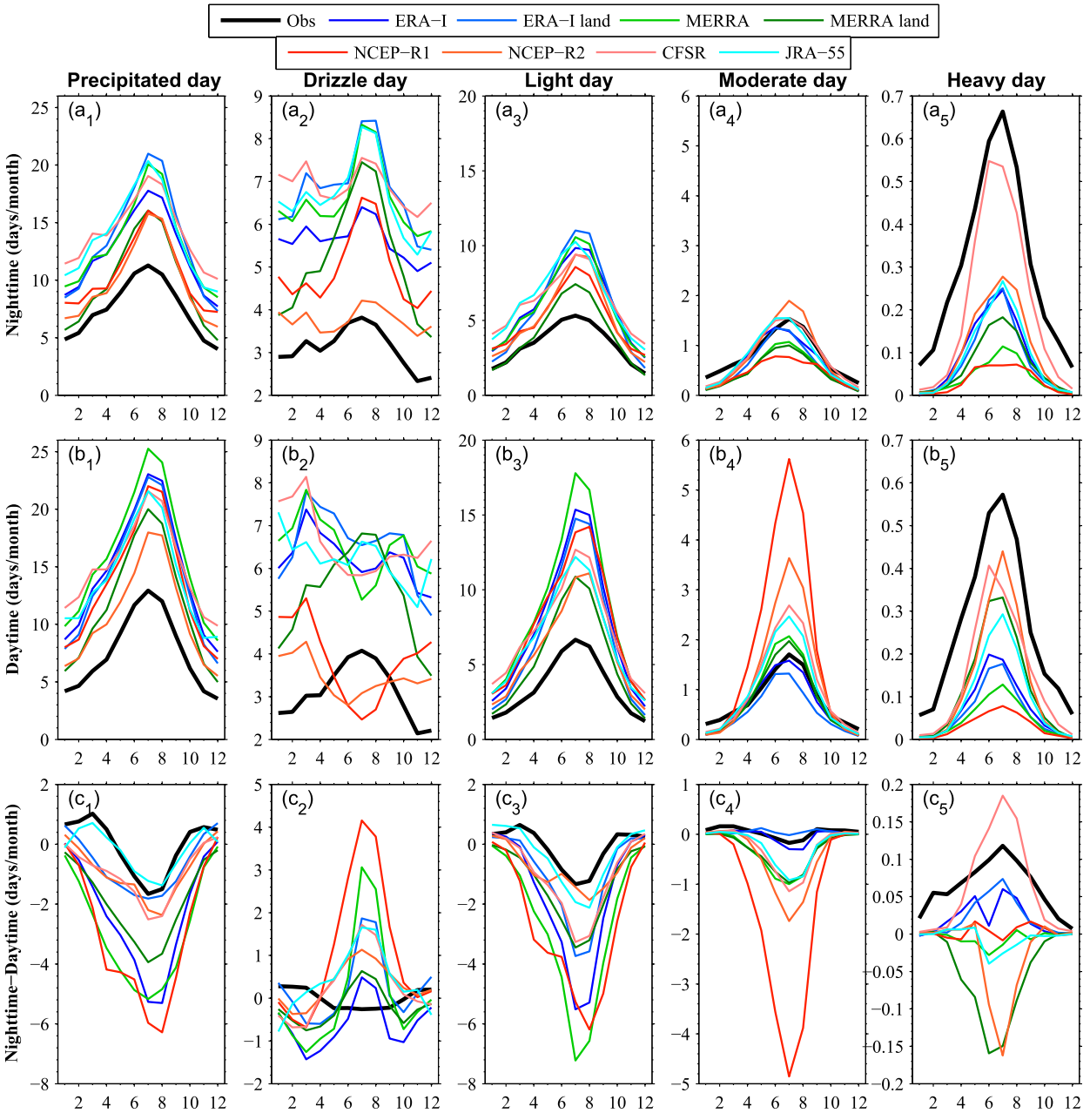

FIG. 4. Seasonal cycles of the (a) nighttime and (b) daytime precipitation frequencies and (c) their differences (nighttime minus daytime; days yr^{-1}) among various precipitation categories over China: that is, (left)–(right) precipitation days [$P \geq 0.1$ mm $(12\ h)^{-1}$], drizzle days [$0.1 \leq P < 1$ mm $(12\ h)^{-1}$], light precipitation days [$1 \leq P < 10$ mm $(12\ h)^{-1}$], moderate precipitation days [$10 \leq P < 25$ mm $(12\ h)^{-1}$], and heavy precipitation days [$P \geq 25$ mm $(12\ h)^{-1}$] from the observed and reanalyzed precipitation datasets. All of the reanalysis datasets overestimate the seasonal cycles of drizzle and light and moderate precipitation frequencies but underestimate the seasonal cycles of heavy precipitation frequencies. The daytime drizzle frequency cannot be reproduced by the reanalysis products.

summer daytime precipitation intensity in the NCEP R1 and NCEP R2 models is related to overestimation of light precipitation intensity (Fig. 6b, left and left center). The reanalysis products roughly exhibit the observed seasonal shape of nighttime–daytime contrast in precipitation intensity over southeastern China (Fig. 5c, left), but not over the other regions. Overall, the reanalysis products present considerable deficiencies in their ability to describe the seasonal cycle of nighttime–daytime contrast in precipitation intensity (Fig. 6c).

A joint comparison of the precipitation frequency and intensity further shows that the seasonal cycle of

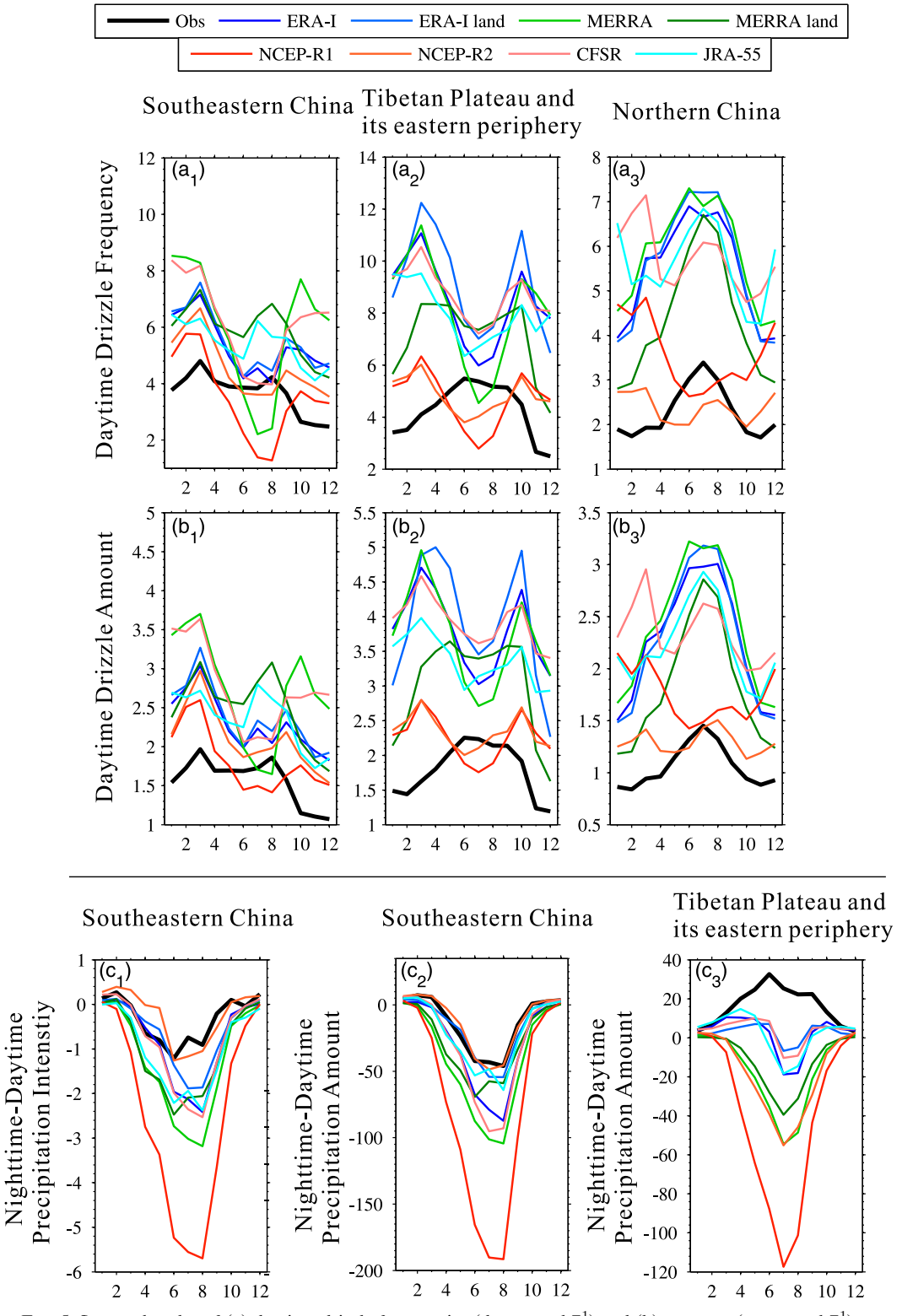

FIG. 5. Seasonal cycles of (a) daytime drizzle frequencies (days month^{-1}) and (b) amounts (mm month^{-1}) over three subregions of China, namely, (left) southeastern China, (center) the Tibetan Plateau and its eastern periphery, and (right) northern China. (c) Nighttime–daytime contrasts of (left) precipitation intensity (mm day^{-1}) and (center) amount (mm month^{-1}) over southeastern China and (right) precipitation amount (mm month^{-1}) over the Tibetan Plateau and its eastern periphery.

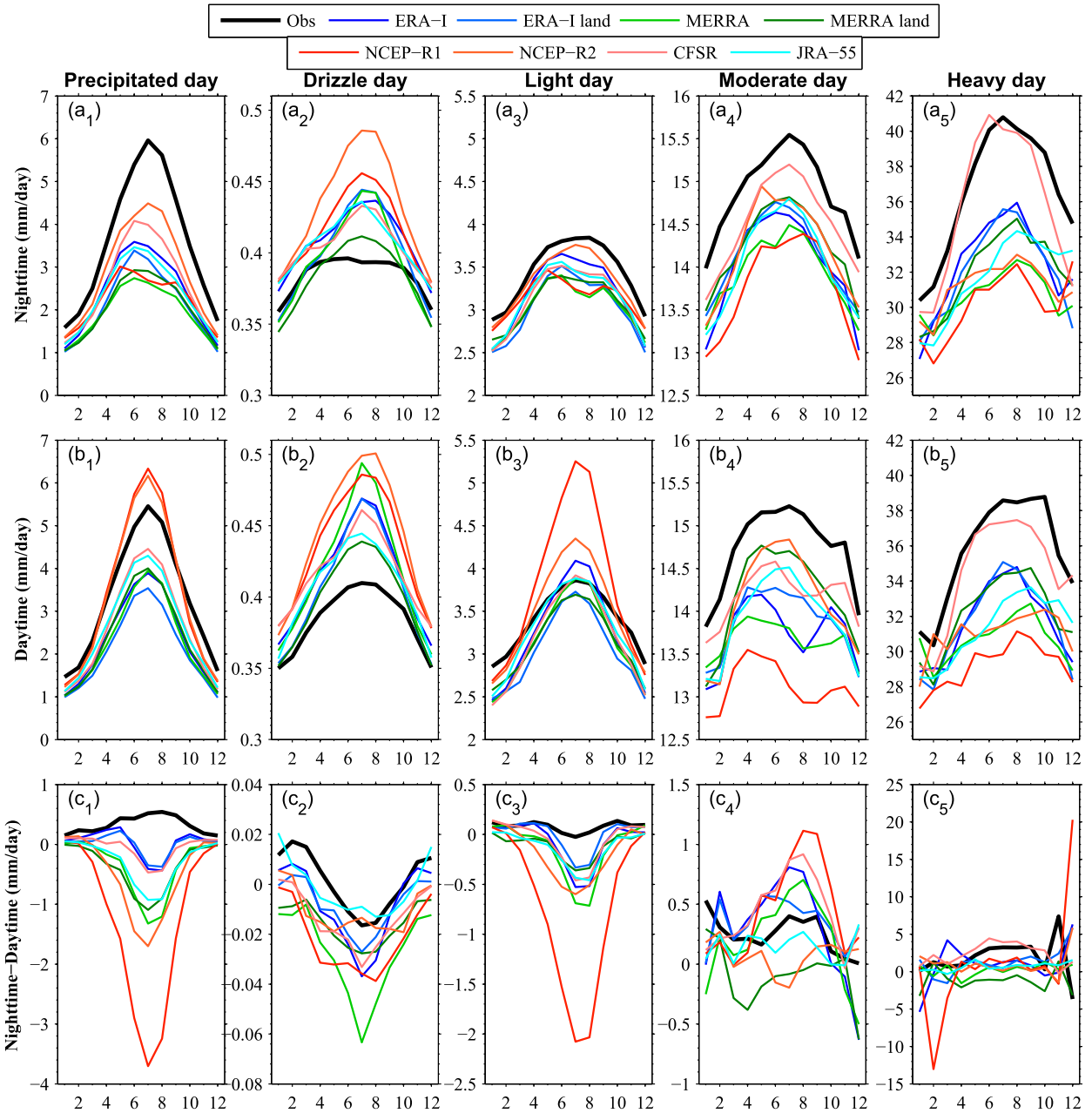

FIG. 6. As in Fig. 4, but for precipitation intensity (mm day^{-1}). The reanalysis products overestimate the seasonal cycles of drizzle intensity and nighttime–daytime contrast in precipitation intensity.

precipitation amount may be largely dominated by the precipitation frequency (Fig. 7), which is similar to the results for monthly precipitation from global climate models (Trenberth et al. 2003; Dai 2006; Sun et al. 2006). Daytime precipitation amount accounts for 48.5% of daily precipitation in the observation but 52.1%–69.9% of daily precipitation in the reanalysis datasets (Fig. 6b, left, and more evident for moderate precipitation in Fig. 6b, right center), which is mainly caused by easily motivated moist convection in the models, especially in summer. However, certain atmospheric processes in nature prevent convective onset, thereby causing substantial water vapor accumulation that leads to daytime heavy precipitation (Trenberth et al. 2003; Dee et al. 2011) and provides sufficient water vapor for nighttime precipitation (Fig. 6). Therefore, schemes of deep convection and associated energetic and moist dynamical processes should be improved.

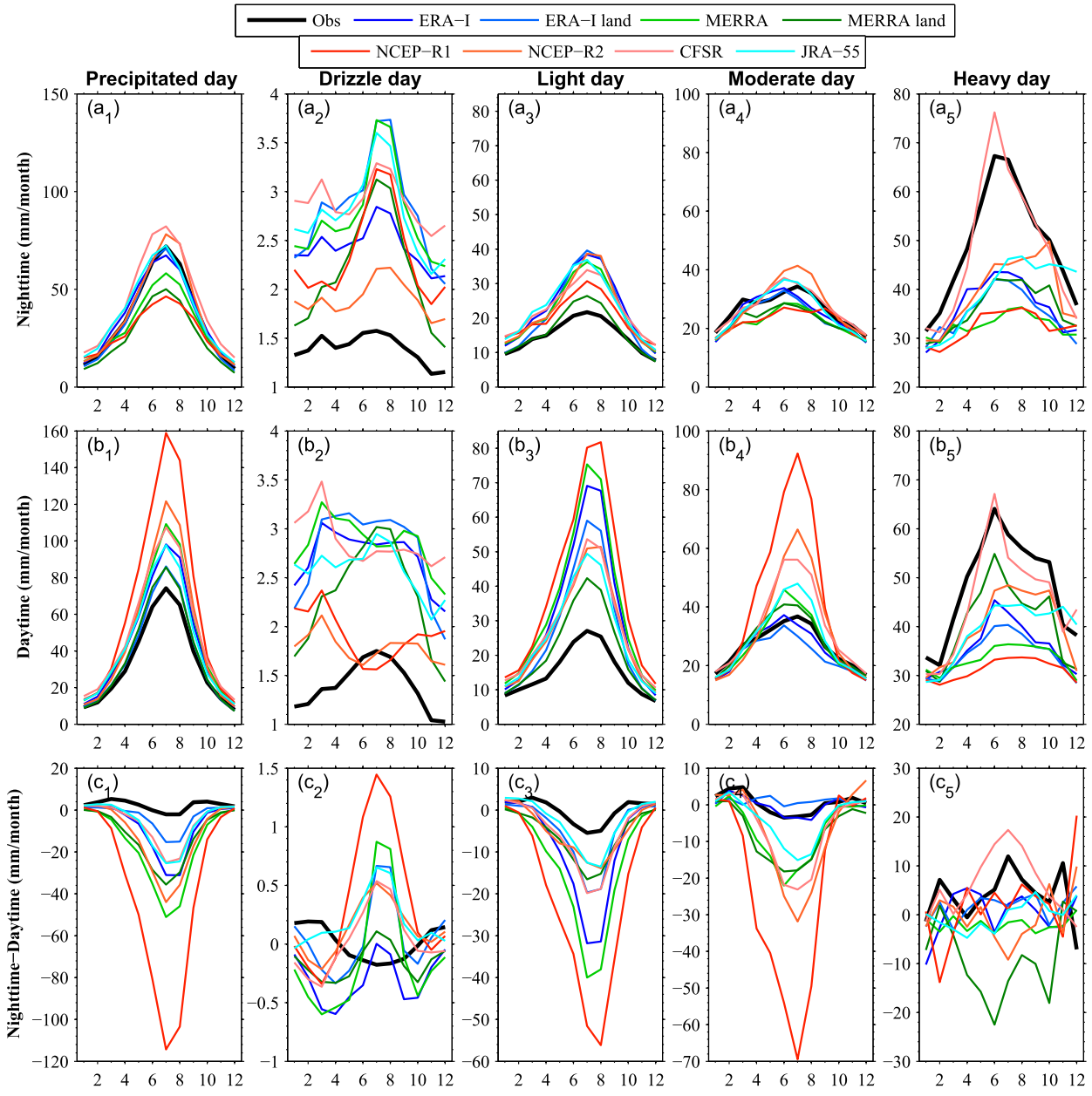

FIG. 7. As in Fig. 4, but for precipitation amount (mm month^{-1}). The results are consistent with those for the frequency, indicating that the seasonal cycles of precipitation amounts are mainly dominated by precipitation frequencies.

The reanalysis products except for MERRA land cannot present the observed seasonal shape of daytime drizzle amount over China (Fig. 7b, left center), mainly due to these products mistakenly reproduce the seasonal shapes over southeastern China and the Tibetan Plateau and its eastern periphery (Figs. 5a,b, left and center). The reanalysis products except for NCEP R1 roughly represent the observed seasonal shape of nighttime–daytime contrast in precipitation amount over southeastern China, despite having certain underestimations (Figs. 2 and 5c, center). The observation exhibits a concave-up seasonal shape of nighttime–daytime contrast in precipitation amount over the Tibetan Plateau and its eastern periphery, whereas the reanalysis products (especially for MERRA, MERRA land, NCEP R1 and NCEP R2) present an opposite shape (Figs. 2 and 5c, right).

c. *Interannual variability of subdaily precipitation*

Figures 8–10 show the time series of nighttime, daytime, and nighttime–daytime contrasts of precipitation

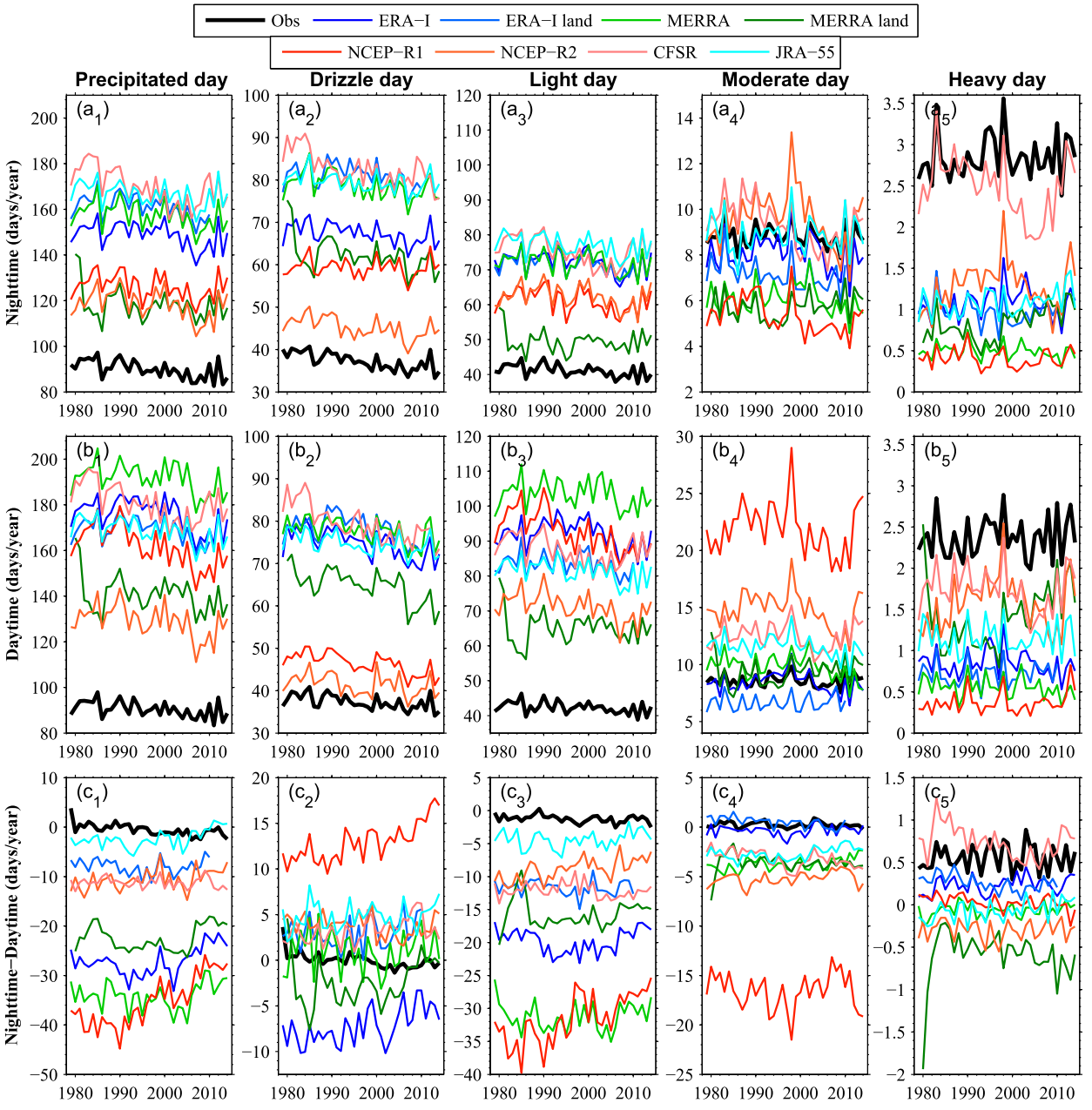

FIG. 8. Time series of the (a) nighttime and (b) daytime precipitation frequencies and (c) nighttime–daytime contrast (nighttime minus daytime; days yr^{-1}) in precipitation frequencies among the different precipitation categories over China: that is, (left)–(right) precipitation days [$P \geq 0.1$ mm $(12\,h)^{-1}$], drizzle days [$0.1 \leq P < 1$ mm $(12\,h)^{-1}$], light precipitation days [$1 \leq P < 10$ mm $(12\,h)^{-1}$], moderate precipitation days [$10 \leq P < 25$ mm $(12\,h)^{-1}$] and heavy precipitation days [$P \geq 25$ mm $(12\,h)^{-1}$] of the observed and reanalyzed precipitation datasets. The spurious error of the MERRA land products in the first two years [i.e., 1980 and 1981 (Fig. 7b, right)] mainly results from a bias in the initial fields of the unified precipitation observations (i.e., the so-called spinup effect).

frequencies, intensities, and amounts among the drizzle and light, moderate, and heavy precipitation categories for the period 1979–2014. Overall, the eight reanalysis datasets can effectively represent the interannual synchronizations (expressed by correlation coefficient) of nighttime and daytime precipitation frequencies and amounts (Figs. 8–10) with a multireanalysis-average correlation coefficient of 0.66 over China (SD = 0.15; Fig. 11), which is consistent with the strong modeling performance for the interannual synchronization of precipitation amount by 18 coupled climate models (Dai 2006) and may indicate a good ability to predict ENSO

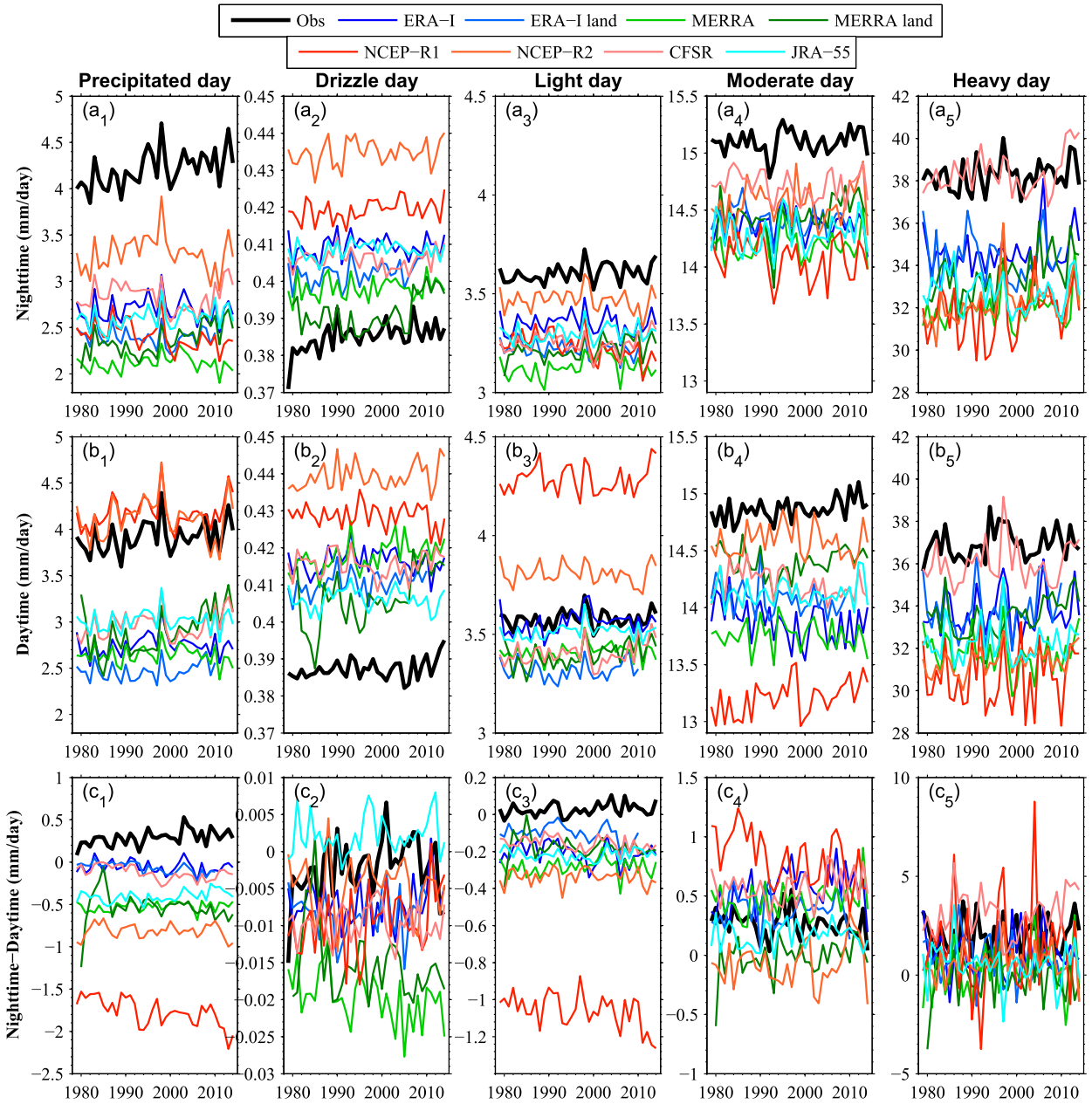

FIG. 9. As in Fig. 8, but for precipitation intensity (mm day^{-1}).

characteristics (Dai and Wigley 2000; Dai 2001a; Hoyos and Webster 2007; Shukla and Kinter 2015).

The reanalysis datasets are able to represent interannual synchronizations of the total and light precipitation intensities over China (Fig. 11). However, they fail to reproduce interannual synchronizations of the drizzle and moderate and heavy precipitation intensities over the Tibetan Plateau and its eastern periphery (Fig. 11). What is more, most reanalysis products have limited abilities to reproduce the interannual synchronizations of nighttime–daytime contrasts in precipitation characteristics, although the ERA-Interim, ERA-Interim/Land, CFSR, and JRA-55 products show some improved performances in certain precipitation categories, especially over southeastern China (Figs. 11a–i, right).

The reanalyses continue to illustrate the modeling ability to simulate interannual amplitudes (expressed by interannual standard deviation) of nighttime, daytime, and nighttime–daytime contrasts in precipitation characteristics. The interannual amplitudes of the nighttime, daytime, and nighttime–daytime contrast in nonheavy precipitation frequencies are overestimated by the eight

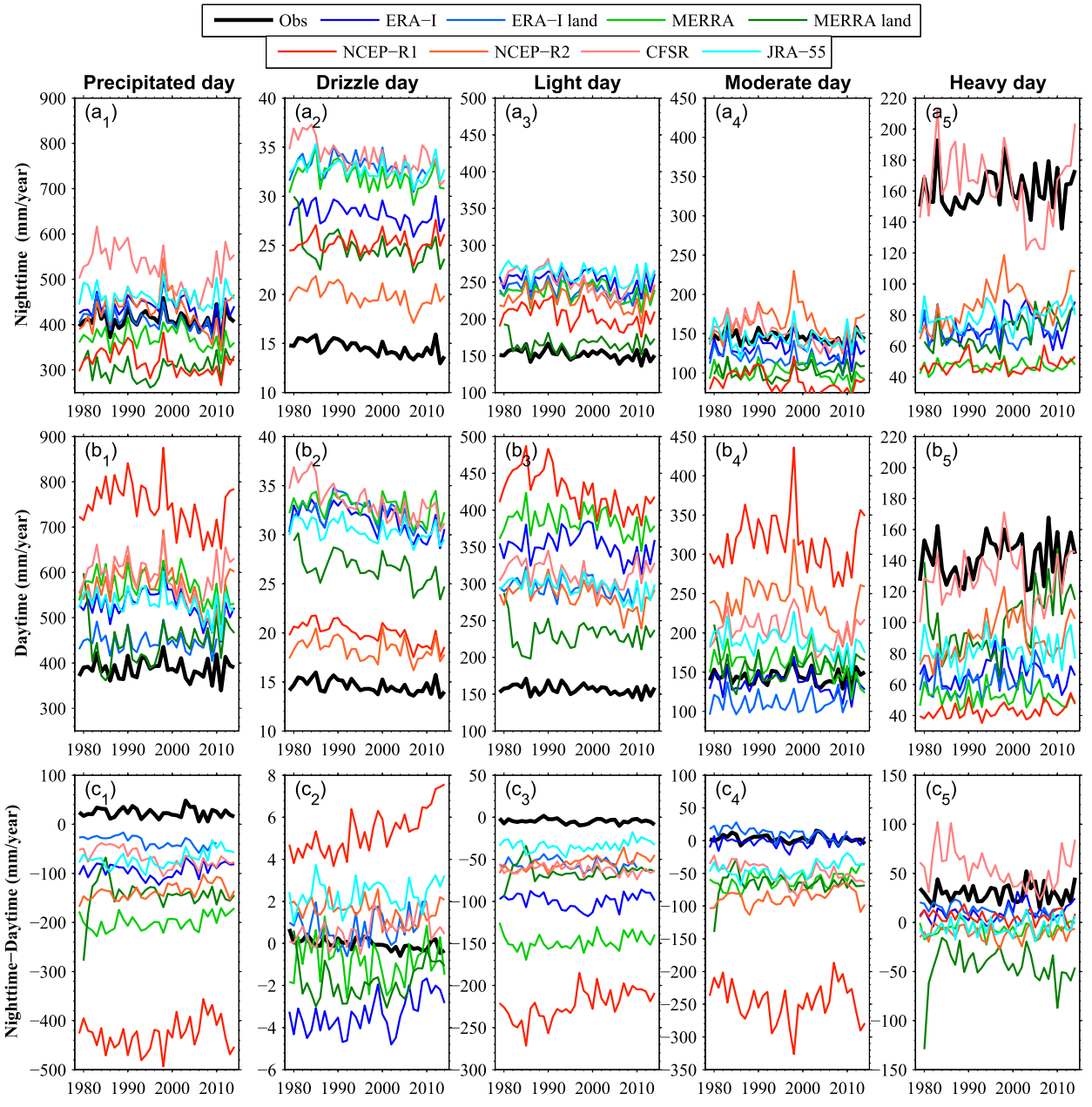

FIG. 10. As in Fig. 8, but for precipitation amount (mm yr^{-1}).

reanalysis datasets (by an average of 53%, 102%, and 101%, respectively), whereas those of heavy precipitation are underestimated over China (Fig. 12a). Similar results happen to precipitation amount (32%, 74%, and 101% for nighttime, daytime, and nighttime–daytime contrast in precipitation amounts, respectively; Fig. 12i). This situation also occurs over the three China subregions (Fig. 12). Additionally, NCEP R1 has the largest overestimated amplitude of nighttime–daytime precipitation contrast (Fig. 12). Additionally, the eight reanalysis products consistently overestimate interannual amplitudes of nighttime, daytime, and nighttime–daytime contrast in nondrizzle precipitation intensities (average of 31%, 32%, and 38% over China, respectively; Figs. 12e–h).

To elucidate the simulated ability of day-to-day variance in precipitation intensity (expressed by standard deviation of nighttime-to-nighttime or daytime-to-daytime precipitation intensity in a year), Fig. 13 further illustrates the multiyear-averaged differences, correlation coefficients, and trends between the observation and reanalysis

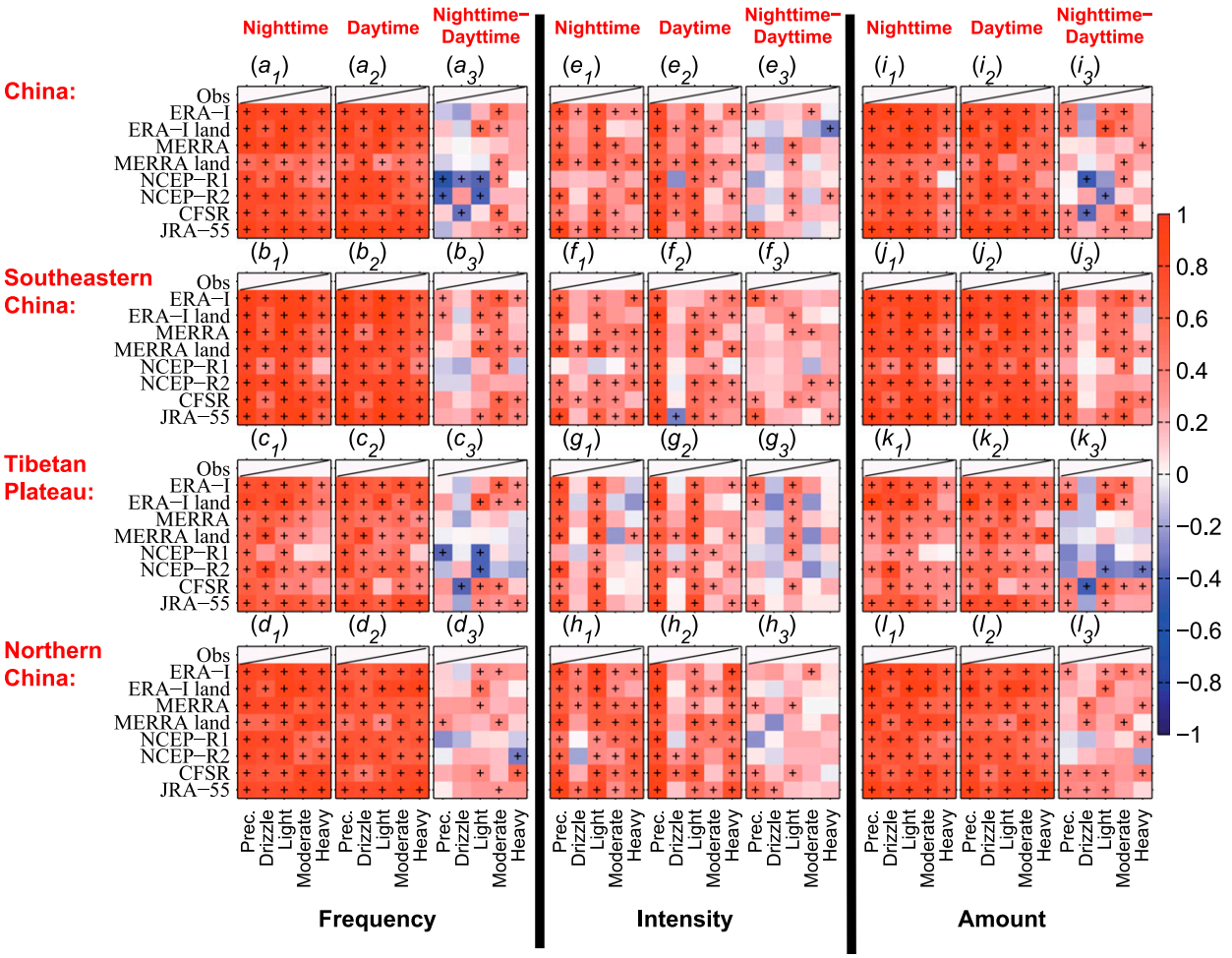

FIG. 11. Interannual correlation coefficients (after detrending) of (left) nighttime, (center) daytime, and (right) nighttime–daytime contrasts in precipitation (a)–(d) frequencies, (e)–(h) intensities, and (i)–(l) amounts between the observed and reanalyzed precipitation datasets. The plus sign denotes the two-tailed Student's t test significance at the 0.05 level.

products. The nighttime-to-nighttime and daytime-to-daytime variances in precipitation intensities are significantly smaller in most of the reanalysis datasets (by an average of −34% and −42% over China and, in particular, −57% and −61% for heavy precipitation intensity) than in the observation (Figs. 13a–d, left and center), likely because of reduced observational constraint involved in these reanalysis models. However, the interannual synchronizations of the nighttime-to-nighttime and daytime-to-daytime variances in nondrizzle precipitation intensities are captured by the reanalysis products, especially over northern China (Figs. 13e–h, left and center).

In the observation, the nighttime-to-nighttime variance in precipitation intensity exhibits a significant trend of 2.0% decade^{-1} during the period 1979–2014 over China that is well captured by JRA-55 (by 2.0% decade^{-1}) and is exaggerated by MERRA land (by 5.0% decade^{-1}), although the other products do not present such a trend (Fig. 13i, left). Over the Tibetan Plateau, such a trend can be captured by most reanalysis products (Fig. 13k, left).

The observed daytime-to-daytime variance in precipitation intensity presents a significant trend of 1.5% decade^{-1} over China, which might be captured by NCEP R1 (1.9% decade^{-1}) and is exaggerated by MERRA land (by 4.1% decade^{-1}; Fig. 13i, right), and this trend over southeastern China is roughly captured by most reanalysis products (Fig. 13j, right). The observed trend in daytime-to-daytime variance of moderate precipitation intensity (0.8% decade^{-1}) is exaggerated by NCEP R1 (2.0% decade^{-1}) over China, although it is underestimated by the other reanalysis products (Fig. 13i, right). The observed trend in daytime-to-daytime variance of heavy precipitation intensity (3.0% decade^{-1}) is exaggerated by MERRA land, NCEP R1, and NCEP R2 (14.1%, 19.5%, and 7.1% decade^{-1} over China,

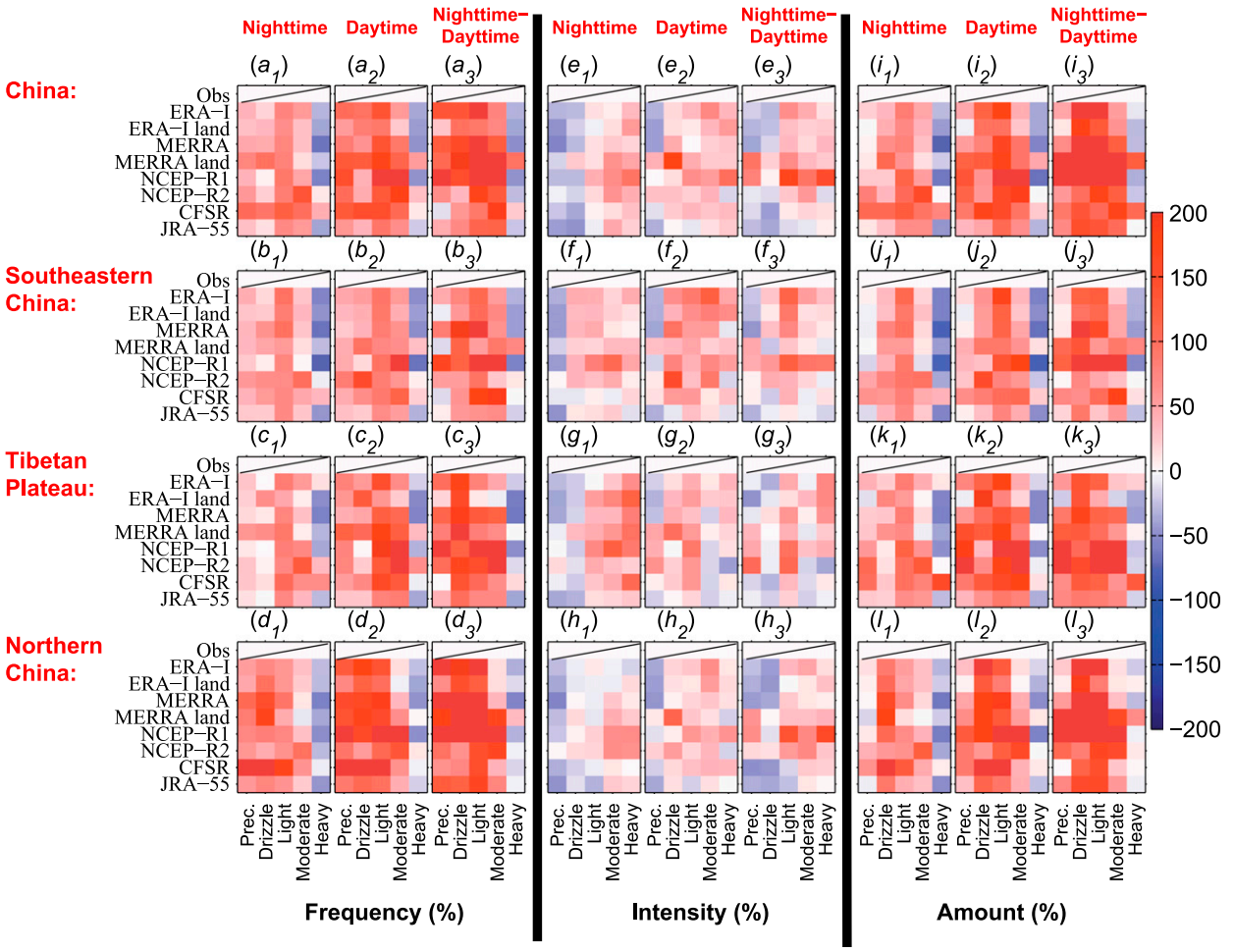

FIG. 12. Normalized differences of the year-to-year SD (%; i.e., reanalysis minus observation divided by the observation multiplied by 100) of the (left) nighttime, (center) daytime, and (right) nighttime–daytime contrasts in precipitation (a)–(d) frequency, (e)–(h) intensity, and (i)–(l) amount anomalies from the eight reanalysis products with respect to the observed SD from 1979 to 2014. The plus sign denotes the two-tailed Student's *t* test significance at the 0.05 level. Year-to-year amplitudes in nighttime, daytime, and nighttime–daytime contrast in nonheavy precipitation frequencies/amounts are overestimated by the eight reanalysis products over China and its three regions, but those in the heavy precipitation group are underestimated.

respectively; Figs. 12 and 13b, right). Therefore, additional efforts should be focused on improving the day-to-day precipitation variability in models.

d. Long-term trends in subdaily precipitation

Because of the anthropogenic greenhouse effect, an asymmetric diurnal warming trend has developed (IPCC 2013; Zhou and Wang 2016b) that further alters the regular diurnal variations of meteorological variables. Moreover, the East Asian summer–winter monsoon has been weakening since the 1980s (Wang 2001; Wang et al. 2009). Presumably, these changes influence the long-term trends of nighttime and daytime precipitation and its partitioning.

Nighttime and daytime precipitation frequencies exhibit significantly downward trends for nonheavy precipitation and nonsignificantly upward trends for heavy precipitation for the period 1979–2014 over China (Figs. 8 and 14a, left and center). Although the eight reanalysis products present large discrepancies in depicting the climatology of precipitation frequency, they exhibit comparative trends in the total, drizzle, and light precipitation frequency with the observed data over China (-2.5%, -3.7%, and -2.0% decade^{-1} during nighttime and -1.7%, -2.4%, and -1.4% decade^{-1} during daytime, respectively; Figs. 8 and 14a, left and center). However, the reanalysis products present limited abilities to represent long-term trends in the moderate and heavy precipitation frequencies (Figs. 8 and 14a, left and center). This situation also happens over southeastern China and northern China (Figs. 14b,d, left and center).

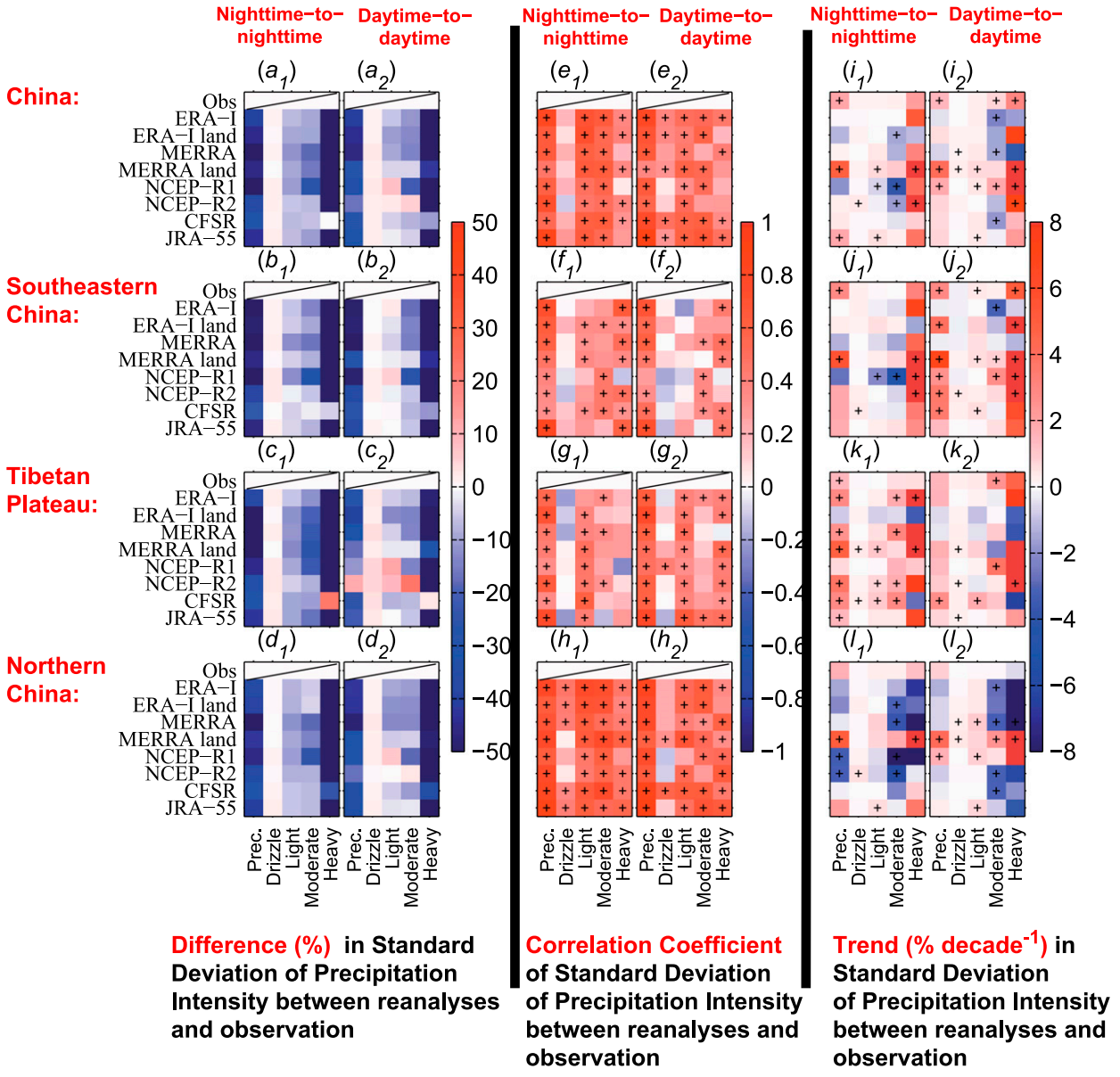

FIG. 13. (a)–(d) Normalized difference (%; i.e., reanalysis minus observation divided by the observation multiplied by 100), (e)–(h) interannual correlation coefficients (after detrending), and (i)–(l) normalized trends (% decade^{-1}) of the (left) nighttime-to-nighttime and (right) daytime-to-daytime SD of precipitation intensities between the observed and reanalyzed products over China and its three subregions: southeastern China, the Tibetan Plateau and its eastern periphery, and northern China. The plus sign denotes the two-tailed Student's *t* test significance at the 0.05 level.

The significant trends in the nighttime–daytime contrasts of precipitation frequencies are observed over China and its three subregions (−0.8%, −1.3%, and −0.6% decade^{-1} for the total, drizzle, and light categories over China, respectively); however, the reanalysis datasets exhibit overall positive trends (Figs. 8 and 14). One exception is that MERRA can reproduce the observed trends in nighttime–daytime contrasts of total and drizzle precipitation frequencies over southeastern China (−0.79% vs −1.27% decade^{-1} and −1.93% vs −2.95% decade^{-1}; Fig. 14b, right). Additionally, the reanalysis products exhibit diverse trends in nighttime–daytime contrasts of moderate and heavy precipitation frequencies over China and its three subregions (Figs. 14a–d, right).

The nighttime and daytime precipitation intensities show significant upward trends for the period 1979–2014 (Figs. 9 and 14). JRA-55 presents a comparative trend in nighttime precipitation intensity (1.4% decade^{-1}) with

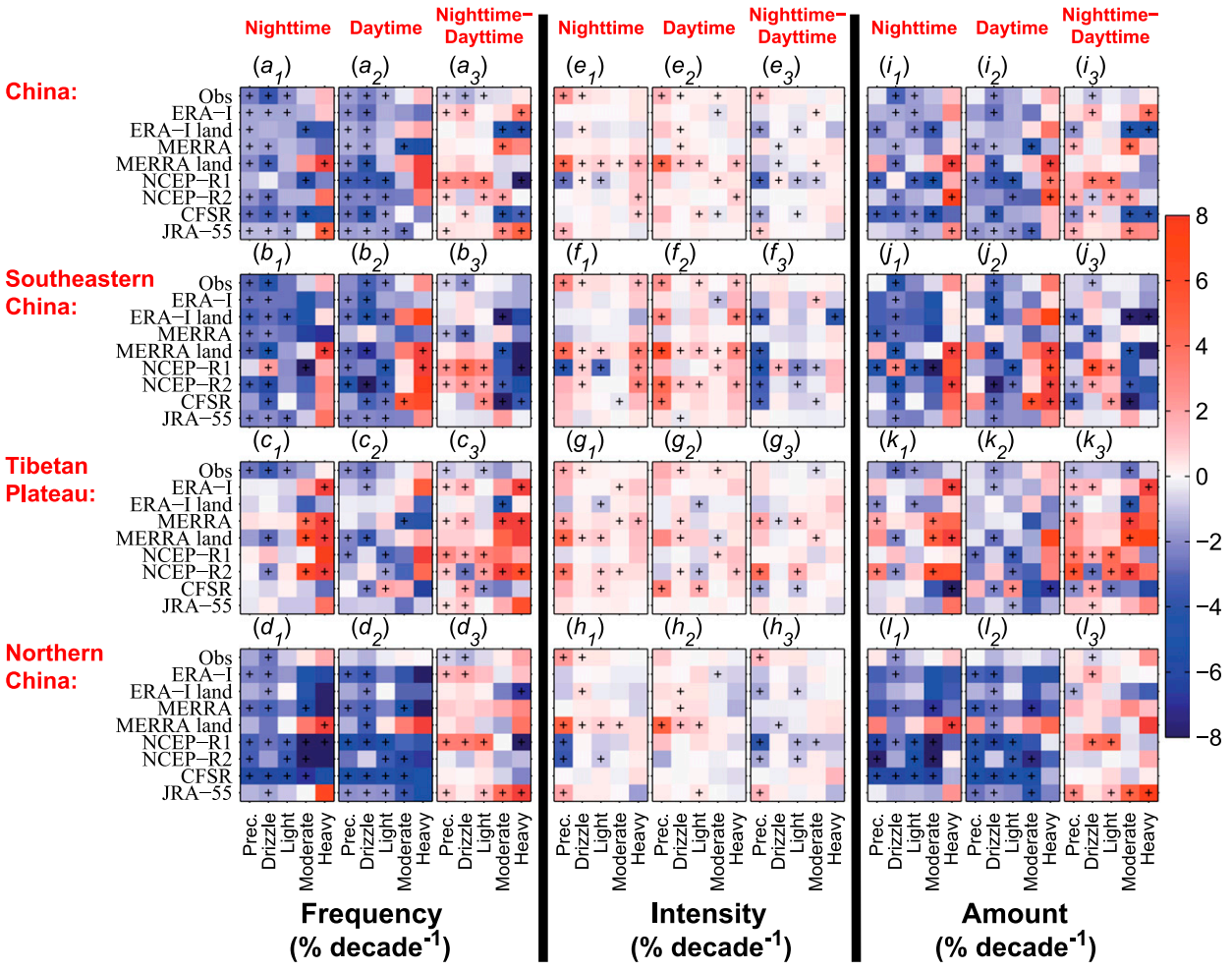

FIG. 14. Normalized trends in the (left) nighttime, (center) daytime, and (right) nighttime–daytime contrasts in precipitation (a)–(d) frequencies, (e)–(h) intensities, and (i)–(l) amounts (% decade^{-1}) from the observed and reanalyzed precipitation datasets over China and its three subregions: southeastern China, the Tibetan Plateau and its eastern periphery, and northern China. The plus sign denotes the two-tailed Student's t test significance at the 0.05 level.

the observed data (2.4% decade^{-1}) over China (Figs. 9 and 14e,h, left and center), and ERA-Interim/Land performs well over southeastern China (2.9% decade^{-1} vs the observed 2.5% decade^{-1}) (Fig. 14f, center). ERA-Interim/Land roughly captures the nighttime and daytime drizzle intensity trends (0.34% and 0.32% decade^{-1} vs the observed 0.52% and 0.24% decade^{-1} over China) (Figs. 9 and 14e,h, left and center). However, MERRA land significantly overestimates the nighttime and daytime precipitation intensity trends over China and its three subregions (4.3% and 4.5% decade^{-1} vs the observed 2.4% and 1.5% decade^{-1} over China; Figs. 9 and 14e–h).

The nighttime–daytime contrast of precipitation intensity presents a significant trend of 1.0% decade^{-1} that is well captured by JRA-55 (0.9% decade^{-1}); however, the other reanalysis datasets exhibit negative trends over China (Figs. 9 and 14e,h, right). Overall, the other reanalysis products have difficulty in depicting the partitioning between nighttime and daytime precipitation intensity in the subcategories (Figs. 9 and 14); therefore, there is considerable room for improvement in depicting long-term trend in diurnal variation of precipitation intensity.

The trends in the nighttime, daytime, and nighttime–daytime contrasts in precipitation amounts are closely (weakly) correlated with those of the precipitation frequencies (intensities), and a multireanalysis-average correlation coefficient of 0.85 (0.26; $p = 0.00$) was generated among all the reanalysis datasets, which indicated that long-term trends in precipitation amounts are dominated by their frequencies (Fig. 14). Nighttime, daytime, and nighttime–daytime contrasts in drizzle precipitation amounts have no significant trends over

China and subregions, but most reanalysis products exhibit diverse significant trends (Figs. 14i–l). Additionally, ERA-Interim/Land and CFSR present negative trends in nighttime–daytime contrasts of precipitation amounts similar to the observed data over the Tibetan Plateau (-1.1% and -2.0% decade^{-1} vs -1.2% decade^{-1}; Fig. 14k, right).

4. Conclusions and discussion

Diurnal precipitation variation is an aspect of multiscale precipitation that is of great importance in terms of hydrological, ecosystem, and climate system regulation. Because purely model-derived precipitation is used in reanalysis products, a multilevel examination of diurnal precipitation variation in models was conducted to provide insights into the model deficiencies in various physical parameterization schemes, including convection triggers, large-scale circulations, and so on. Nighttime and daytime precipitation data from approximately 2100 meteorological stations for the period 1979–2014 over China were used to comprehensively examine the performance of old- and new-generation reanalysis products in capturing the characteristics of diurnal precipitation variation, including the climatology, seasonal cycle, interannual variability, and long-term trends.

Our results indicate that the observed nighttime–daytime precipitation contrast exhibits an evident dipole field, with a positive center over the Tibetan Plateau and its eastern periphery and a negative center over southeastern China. ERA-Interim, ERA-Interim/Land, JRA-55, and CFSR roughly capture the dipole pattern, albeit with underestimations of the positive and negative centers; however, MERRA, MERRA land, NCEP R1, and NCEP R2 do not capture this pattern. This representation of the dipole pattern of nighttime–daytime precipitation contrast reflects skillful parameterizations of topography-related treatments and large-scale breeze circulations.

The eight reanalysis products can represent the seasonal shapes of nighttime and daytime precipitation frequencies except for the daytime drizzle frequency. However, the total precipitation frequencies are overestimated by 31.5%–88.7% during nighttime and 42.7%–111.8% during daytime, and the heavy precipitation frequency is underestimated by greater than 30.8% in all the reanalysis datasets. In NCEP R1, NCEP R2, and CFSR, a large overestimation of the summer daytime moderate precipitation frequency makes the summer daytime drizzle occur infrequently. These results reveal the relatively easy and frequent start of moist convection in the reanalysis models and the resulting overestimation of shallow convective precipitation during the daytime. These results further extend previous results that revealed an overestimation of the precipitation frequency of >14.8 mm day^{-1} by NCEP R2 (Huang et al. 2016) and underestimation by ERA-Interim (de Leeuw et al. 2015).

Most reanalysis products (except for NCEP R1 and NCEP R2) underestimate nondrizzle precipitation intensity and overestimate drizzle intensity. A joint comparison of the precipitation frequency and intensity shows that the seasonal cycle of precipitation amount is largely dominated by the precipitation frequency. The overly frequent precipitation at a reduced intensity and infrequent heavy precipitation in the reanalyzed models likely have vital impacts on the partitioning of precipitation into soil moisture and runoff.

The eight reanalysis products can effectively represent the interannual synchronizations of the nighttime and daytime precipitation frequencies and amounts. However, most of the reanalysis products have limited abilities to reproduce the interannual synchronizations of nighttime–daytime contrasts in precipitation characteristics. Most of the reanalysis products exaggerate the year-to-year precipitation variability, although they show significantly narrower day-to-day precipitation variabilities in light, moderate, and heavy precipitation categories.

Most reanalysis products cannot capture the observed trend (2.0% decade^{-1}) in nighttime-to-nighttime variance in precipitation intensity, except for JRA-55 (by 2.0% decade^{-1}) and MERRA land (by 5.0% decade^{-1}). The observed daytime-to-daytime variance in precipitation intensity presents a significant trend of 1.5% decade^{-1}, which might be captured by NCEP R1 (1.9% decade^{-1}) and is exaggerated by MERRA land (by 4.1% decade^{-1}). Additionally, most reanalysis products mistakenly exhibit significant positive trends in nighttime-to-nighttime variations in heavy precipitation intensities over the Tibetan Plateau, despite no significant trend in the observation. Therefore, additional efforts should be focused on improving the day-to-day precipitation variability in models.

The observation shows that the nighttime and daytime precipitation frequencies exhibit significant downward trends, which are roughly captured by all the reanalysis products. The trends in precipitation amounts are dominated by those of precipitation frequencies, so a similar situation happens to precipitation amounts in reanalysis models. This result is consistent with that based on daily precipitation (Zhou and Wang 2017). Nighttime and daytime precipitation intensities show significant upward trends during the period 1979–2014. Only JRA-55 shows a comparative trend in nighttime precipitation intensity (1.4% decade^{-1}) with the observed data (2.4% decade^{-1}), and the other products exhibit negative trends.

The significant trends in nighttime–daytime contrasts of precipitation frequencies are observed for the total (-0.8% decade^{-1}), drizzle (-1.3% decade^{-1}), and light (-0.6% decade^{-1}) categories, but most of the reanalysis products exhibit overall positive trends. Most of the reanalyses have difficulty in depicting the long-term partitioning between nighttime and daytime precipitation in the subcategories. Therefore, the reanalysis products have considerable room for improvement in depicting long-term trend in diurnal precipitation variation, including their response to the asymmetrical warming, atmospheric circulation related to complex topography, and so on (Chen and Houze 1997; Trenberth et al. 2003; Dai 2006).

Instead of harmonic phase analysis (Yu et al. 2007a; Yuan et al. 2013), methodology on separation into daytime, nighttime, and nighttime–daytime contrast of precipitation proposed in this study can be applied to satellite-based observations in spite of just several samplings daily. This helps to examine many processes of precipitation characteristics (e.g., the asymmetric trends in daytime and nighttime precipitation) by the use of station- and satellite-based observations.

Acknowledgments. This study was funded by the National Natural Science Foundation of China (41525018 and 91337111) and the National Basic Research Program of China (2017YFA0603601). The latest precipitation data were obtained from the China Meteorological Administration (CMA). Considerable gratitude is owed to several reanalysis working teams, including the European Centre for Medium-Range Weather Forecasts (ECMWF) for providing ERA-Interim and ERA-Interim/Land data; the Global Modeling and Assimilation Office (GMAO) at the NASA Goddard Space Flight Center (GSFC) for MERRA and MERRA land data; the NOAA/Earth System Research Laboratory (ESRL) for NCEP R1, NCEP R2, and CFSR data; and the Climate Prediction Division of the Global Environment and Marine Department at the Japan Meteorological Agency (JMA) for JRA-55 data (http://jra.kishou.go.jp/). We thank the United States Geological Survey Earth Resources Observation and Science Data Center for GTOPO30 (https://lta.cr.usgs.gov/GTOPO30).

REFERENCES

Alexandersson, H., 1986: A homogeneity test applied to precipitation data. *J. Climatol.*, **6**, 661–675, doi:10.1002/joc.3370060607.

Ashouri, H., K.-L. Hsu, S. Sorooshian, D. K. Braithwaite, K. R. Knapp, L. D. Cecil, B. R. Nelson, and O. P. Prat, 2015: PERSIANN-CDR: Daily precipitation climate data record from multisatellite observations for hydrological and climate studies. *Bull. Amer. Meteor. Soc.*, **96**, 69–83, doi:10.1175/BAMS-D-13-00068.1.

——, S. Sorooshian, K.-L. Hsu, M. G. Bosilovich, J. Lee, M. F. Wehner, and A. Collow, 2016: Evaluation of NASA's MERRA precipitation product in reproducing the observed trend and distribution of extreme precipitation events in the United States. *J. Hydrometeor.*, **17**, 693–711, doi:10.1175/JHM-D-15-0097.1.

Balsamo, G., and Coauthors, 2015: ERA-Interim/Land: A global land surface reanalysis data set. *Hydrol. Earth Syst. Sci.*, **19**, 389–407, doi:10.5194/hess-19-389-2015.

Betts, A. K., and C. Jakob, 2002: Evaluation of the diurnal cycle of precipitation, surface thermodynamics, and surface fluxes in the ECMWF model using LBA data. *J. Geophys. Res.*, **107**, LBA 12-1–LBA 12-8, doi:10.1029/2001JD000427.

Bosilovich, M. G., J. Chen, F. R. Robertson, and R. F. Adler, 2008: Evaluation of global precipitation in reanalyses. *J. Appl. Meteor. Climatol.*, **47**, 2279–2299, doi:10.1175/2008JAMC1921.1.

Chen, G., W. Sha, and T. Iwasaki, 2009: Diurnal variation of precipitation over southeastern China: Spatial distribution and its seasonality. *J. Geophys. Res.*, **114**, D13103, doi:10.1029/2008JD011103.

——, T. Iwasaki, H. Qin, and W. Sha, 2014: Evaluation of the warm-season diurnal variability over East Asia in recent reanalyses JRA-55, ERA-Interim, NCEP CFSR, and NASA MERRA. *J. Climate*, **27**, 5517–5537, doi:10.1175/JCLI-D-14-00005.1.

Chen, H., W. Yuan, J. Li, and R. Yu, 2012: A possible cause for different diurnal variations of warm season rainfall as shown in station observations and TRMM 3B42 data over the southeastern Tibetan Plateau. *Adv. Atmos. Sci.*, **29**, 193–200, doi:10.1007/s00376-011-0218-1.

Chen, M., W. Shi, P. Xie, V. Silva, V. E. Kousky, R. Wayne Higgins, and J. E. Janowiak, 2008: Assessing objective techniques for gauge-based analyses of global daily precipitation. *J. Geophys. Res.*, **113**, D04110, doi:10.1029/2007JD009132.

Chen, S. S., and R. A. Houze, 1997: Diurnal variation and life-cycle of deep convective systems over the tropical Pacific warm pool. *Quart. J. Roy. Meteor. Soc.*, **123**, 357–388, doi:10.1002/qj.49712353806.

Chow, K. C., and J. C. L. Chan, 2009: Diurnal variations of circulation and precipitation in the vicinity of the Tibetan Plateau in early summer. *Climate Dyn.*, **32**, 55–73, doi:10.1007/s00382-008-0374-x.

Dai, A., 2001a: Global precipitation and thunderstorm frequencies. Part I: Seasonal and interannual variations. *J. Climate*, **14**, 1092–1111, doi:10.1175/1520-0442(2001)014<1092:GPATFP>2.0.CO;2.

——, 2001b: Global precipitation and thunderstorm frequencies. Part II: Diurnal variations. *J. Climate*, **14**, 1112–1128, doi:10.1175/1520-0442(2001)014<1112:GPATFP>2.0.CO;2.

——, 2006: Precipitation characteristics in eighteen coupled climate models. *J. Climate*, **19**, 4605–4630, doi:10.1175/JCLI3884.1.

——, and C. Deser, 1999: Diurnal and semidiurnal variations in global surface wind and divergence fields. *J. Geophys. Res.*, **104**, 31 109–31 125, doi:10.1029/1999JD900927.

——, and J. Wang, 1999: Diurnal and semidiurnal tides in global surface pressure fields. *J. Atmos. Sci.*, **56**, 3874–3891, doi:10.1175/1520-0469(1999)056<3874:DASTIG>2.0.CO;2.

——, and T. M. L. Wigley, 2000: Global patterns of ENSO-induced precipitation. *Geophys. Res. Lett.*, **27**, 1283–1286, doi:10.1029/1999GL011140.

——, F. Giorgi, and K. E. Trenberth, 1999: Observed and model-simulated diurnal cycles of precipitation over the contiguous United States. *J. Geophys. Res.*, **104**, 6377–6402, doi:10.1029/98JD02720.

Dee, D. P., and Coauthors, 2011: The ERA-Interim reanalysis: Configuration and performance of the data assimilation system. *Quart. J. Roy. Meteor. Soc.*, **137**, 553–597, doi:10.1002/qj.828.

——, M. Balmaseda, G. Balsamo, R. Engelen, A. J. Simmons, and J. N. Thépaut, 2014: Toward a consistent reanalysis of the climate system. *Bull. Amer. Meteor. Soc.*, **95**, 1235–1248, doi:10.1175/BAMS-D-13-00043.1.

de Leeuw, J., J. Methven, and M. Blackburn, 2015: Evaluation of ERA-Interim reanalysis precipitation products using England and Wales observations. *Quart. J. Roy. Meteor. Soc.*, **141**, 798–806, doi:10.1002/qj.2395.

Deshpande, N. R., and B. N. Goswami, 2014: Modulation of the diurnal cycle of rainfall over India by intraseasonal variations of Indian summer monsoon. *Int. J. Climatol.*, **34**, 793–807, doi:10.1002/joc.3719.

Habib, E., A. T. Haile, Y. Tian, and R. J. Joyce, 2012: Evaluation of the high-resolution CMORPH satellite rainfall product using dense rain gauge observations and radar-based estimates. *J. Hydrometeor.*, **13**, 1784–1798, doi:10.1175/JHM-D-12-017.1.

Houze, R. A., 2012: Orographic effects on precipitating clouds. *Rev. Geophys.*, **50**, RG1001, doi:10.1029/2011RG000365.

Hoyos, C. D., and P. J. Webster, 2007: The role of intraseasonal variability in the nature of Asian monsoon precipitation. *J. Climate*, **20**, 4402–4424, doi:10.1175/JCLI4252.1.

Huang, D.-Q., J. Zhu, Y.-C. Zhang, Y. Huang, and X.-Y. Kuang, 2016: Assessment of summer monsoon precipitation derived from five reanalysis datasets over East Asia. *Quart. J. Roy. Meteor. Soc.*, **142**, 108–119, doi:10.1002/qj.2634.

Huffman, G. J., and Coauthors, 1997: The Global Precipitation Climatology Project (GPCP) combined precipitation dataset. *Bull. Amer. Meteor. Soc.*, **78**, 5–20, doi:10.1175/1520-0477(1997)078<0005:TGPCPG>2.0.CO;2.

——, and Coauthors, 2007: The TRMM Multisatellite Precipitation Analysis (TMPA): Quasi-global, multiyear, combined-sensor precipitation estimates at fine scales. *J. Hydrometeor.*, **8**, 38–55, doi:10.1175/JHM560.1.

IPCC, 2013: *Climate Change 2013: The Physical Science Basis*. Cambridge University Press, 1535 pp., doi:10.1017/CBO9781107415324.

Kalnay, E., and Coauthors, 1996: The NCEP/NCAR 40-Year Reanalysis Project. *Bull. Amer. Meteor. Soc.*, **77**, 437–471, doi:10.1175/1520-0477(1996)077<0437:TNYRP>2.0.CO;2.

Kanamitsu, M., W. Ebisuzaki, J. Woollen, S.-K. Yang, J. J. Hnilo, M. Fiorino, and G. L. Potter, 2002: NCEP–DOE AMIP-II Reanalysis (R-2). *Bull. Amer. Meteor. Soc.*, **83**, 1631–1643, doi:10.1175/BAMS-83-11-1631.

Kobayashi, S., and Coauthors, 2015: The JRA-55 reanalysis: General specifications and basic characteristics. *J. Meteor. Soc. Japan*, **93**, 5–48, doi:10.2151/jmsj.2015-001.

Lin, R., T. Zhou, and Y. Qian, 2014: Evaluation of global monsoon precipitation changes based on five reanalysis datasets. *J. Climate*, **27**, 1271–1289, doi:10.1175/JCLI-D-13-00215.1.

Lin, X., D. A. Randall, and L. D. Fowler, 2000: Diurnal variability of the hydrologic cycle and radiative fluxes: Comparisons between observations and a GCM. *J. Climate*, **13**, 4159–4179, doi:10.1175/1520-0442(2000)013<4159:DVOTHC>2.0.CO;2.

Liu, X., A. Bai, and C. Liu, 2009: Diurnal variations of summertime precipitation over the Tibetan Plateau in relation to orographically-induced regional circulations. *Environ. Res. Lett.*, **4**, 045203, doi:10.1088/1748-9326/4/4/045203.

Ma, S., T. Zhou, A. Dai, and Z. Han, 2015: Observed changes in the distributions of daily precipitation frequency and amount over China from 1960 to 2013. *J. Climate*, **28**, 6960–6978, doi:10.1175/JCLI-D-15-0011.1.

Miao, C., H. Ashouri, K.-L. Hsu, S. Sorooshian, and Q. Duan, 2015: Evaluation of the PERSIANN-CDR daily rainfall estimates in capturing the behavior of extreme precipitation events over China. *J. Hydrometeor.*, **16**, 1387–1396, doi:10.1175/JHM-D-14-0174.1.

Nesbitt, S. W., and E. J. Zipser, 2003: The diurnal cycle of rainfall and convective intensity according to three years of TRMM measurements. *J. Climate*, **16**, 1456–1475, doi:10.1175/1520-0442-16.10.1456.

Oki, T., and K. Musiake, 1994: Seasonal change of the diurnal cycle of precipitation over Japan and Malaysia. *J. Appl. Meteor.*, **33**, 1445–1463, doi:10.1175/1520-0450(1994)033<1445:SCOTDC>2.0.CO;2.

Pinker, R. T., Y. Zhao, C. Akoshile, J. Janowiak, and P. Arkin, 2006: Diurnal and seasonal variability of rainfall in the sub-Sahel as seen from observations, satellites and a numerical model. *Geophys. Res. Lett.*, **33**, L07806, doi:10.1029/2005GL025192.

Poveda, G., and Coauthors, 2005: The diurnal cycle of precipitation in the tropical Andes of Colombia. *Mon. Wea. Rev.*, **133**, 228–240, doi:10.1175/MWR-2853.1.

Randall, D. A., Harshvardhan, and D. A. Dazlich, 1991: Diurnal variability of the hydrologic cycle in a general circulation model. *J. Atmos. Sci.*, **48**, 40–62, doi:10.1175/1520-0469(1991)048<0040:DVOTHC>2.0.CO;2.

Reichle, R. H., R. D. Koster, G. J. M. De Lannoy, B. A. Forman, Q. Liu, S. P. P. Mahanama, and A. Touré, 2011: Assessment and enhancement of MERRA land surface hydrology estimates. *J. Climate*, **24**, 6322–6338, doi:10.1175/JCLI-D-10-05033.1.

Ren, Z. H., and Coauthors, 2010: Quality control procedures for hourly precipitation data from automatic weather stations in China (in Chinese). *Meteor. Mon.*, **36**, 123–132.

Rienecker, M. M., and Coauthors, 2011: MERRA: NASA's Modern-Era Retrospective Analysis for Research and Applications. *J. Climate*, **24**, 3624–3648, doi:10.1175/JCLI-D-11-00015.1.

Saha, S., and Coauthors, 2010: The NCEP Climate Forecast System Reanalysis. *Bull. Amer. Meteor. Soc.*, **91**, 1015–1057, doi:10.1175/2010BAMS3001.1.

Schneider, T., P. A. O'Gorman, and X. J. Levine, 2010: Water vapor and the dynamics of climate changes. *Rev. Geophys.*, **48**, RG3001, doi:10.1029/2009RG000302.

Shen, Y., and A. Xiong, 2016: Validation and comparison of a new gauge-based precipitation analysis over mainland China. *Int. J. Climatol.*, **36**, 252–265, doi:10.1002/joc.4341.

Shukla, R. P., and J. L. Kinter, 2015: Simulations of the Asian monsoon using a regionally coupled-global model. *Climate Dyn.*, **44**, 827–843, doi:10.1007/s00382-014-2188-3.

Silva Dias, P. L., J. P. Bonatti, and V. E. Kousky, 1987: Diurnally forced tropical tropospheric circulation over South America. *Mon. Wea. Rev.*, **115**, 1465–1478, doi:10.1175/1520-0493(1987)115<1465:DFTTCO>2.0.CO;2.

Singh, P., and K. Nakamura, 2009: Diurnal variation in summer precipitation over the central Tibetan Plateau. *J. Geophys. Res.*, **114**, D20107, doi:10.1029/2009JD011788.

Sui, C. H., K. M. Lau, Y. N. Takayabu, and D. A. Short, 1997: Diurnal variations in tropical oceanic cumulus convection during TOGA COARE. *J. Atmos. Sci.*, **54**, 639–655, doi:10.1175/1520-0469(1997)054<0639:DVITOC>2.0.CO;2.

Sun, Y., S. Solomon, A. Dai, and R. W. Portmann, 2006: How often does it rain? *J. Climate*, **19**, 916–934, doi:10.1175/JCLI3672.1.

Trenberth, K. E., A. Dai, R. M. Rasmussen, and D. B. Parsons, 2003: The changing character of precipitation. *Bull. Amer. Meteor. Soc.*, **84**, 1205–1217, doi:10.1175/BAMS-84-9-1205.

Wallace, J. M., 1975: Diurnal variations in precipitation and thunderstorm frequency over the conterminous United States. *Mon. Wea. Rev.*, **103**, 406–419, doi:10.1175/1520-0493(1975)103<0406:DVIPAT>2.0.CO;2.

Wang, A., and X. Zeng, 2012: Evaluation of multireanalysis products with in situ observations over the Tibetan Plateau. *J. Geophys. Res.*, **117**, D05102, doi:10.1029/2011JD016553.

Wang, H., 2001: The weakening of the Asian monsoon circulation after the end of 1970's. *Adv. Atmos. Sci.*, **18**, 376–386, doi:10.1007/BF02919316.

Wang, L., R. Huang, L. Gu, W. Chen, and L. Kang, 2009: Interdecadal variations of the East Asian winter monsoon and their association with quasi-stationary planetary wave activity. *J. Climate*, **22**, 4860–4872, doi:10.1175/2009JCLI2973.1.

Xie, P., M. Chen, S. Yang, A. Yatagai, T. Hayasaka, Y. Fukushima, and C. Liu, 2007: A gauge-based analysis of daily precipitation over East Asia. *J. Hydrometeor.*, **8**, 607–626, doi:10.1175/JHM583.1.

Xu, K.-M., and D. A. Randall, 1995: Impact of interactive radiative transfer on the macroscopic behavior of cumulus ensembles. Part II: Mechanisms for cloud–radiation interactions. *J. Atmos. Sci.*, **52**, 800–817, doi:10.1175/1520-0469(1995)052<0800:IOIRTO>2.0.CO;2.

Yin, X., A. Gruber, and P. Arkin, 2004: Comparison of the GPCP and CMAP merged gauge–satellite monthly precipitation products for the period 1979–2001. *J. Hydrometeor.*, **5**, 1207–1222, doi:10.1175/JHM-392.1.

You, Q. L., J. Z. Min, W. Zhang, N. Pepin, and S. C. Kang, 2015: Comparison of multiple datasets with gridded precipitation observations over the Tibetan Plateau. *Climate Dyn.*, **45**, 791–806, doi:10.1007/s00382-014-2310-6.

Yu, R., Y. Xu, T. Zhou, and J. Li, 2007a: Relation between rainfall duration and diurnal variation in the warm season precipitation over central eastern China. *Geophys. Res. Lett.*, **34**, L13703, doi:10.1029/2007GL030315.

——, T. Zhou, A. Xiong, Y. Zhu, and J. Li, 2007b: Diurnal variations of summer precipitation over contiguous China. *Geophys. Res. Lett.*, **34**, L01704, doi:10.1029/2006GL028129.

——, W. Yuan, J. Li, and Y. Fu, 2010: Diurnal phase of late-night against late-afternoon of stratiform and convective precipitation in summer southern contiguous China. *Climate Dyn.*, **35**, 567–576, doi:10.1007/s00382-009-0568-x.

Yuan, W., R. Yu, and J. Li, 2013: Changes in the diurnal cycles of precipitation over eastern China in the past 40 years. *Adv. Atmos. Sci.*, **30**, 461–467, doi:10.1007/s00376-012-2092-x.

Zhou, C., and K. Wang, 2016a: Spatiotemporal divergence of the warming hiatus over land based on different definitions of mean temperature. *Sci. Rep.*, **6**, 31 789, doi:10.1038/srep31789.

——, and ——, 2016b: Coldest temperature extreme monotonically increased and hottest extreme oscillated over Northern Hemisphere land during last 114 years. *Sci. Rep.*, **6**, 25 721, doi:10.1038/srep25721.

——, and ——, 2016c: Land surface temperature over global deserts: Means, variability, and trends. *J. Geophys. Res. Atmos.*, **121**, 14 344–14 357, doi:10.1002/2016JD025410.

——, and ——, 2017: Quantifying the sensitivity of precipitation to the long-term warming trend and interannual-decadal variation of surface air temperature over China. *J. Climate*, **30**, 3687–3703, doi:10.1175/JCLI-D-16-0515.1.

Zhuo, H., P. Zhao, and T. Zhou, 2014: Diurnal cycle of summer rainfall in Shandong of eastern China. *Int. J. Climatol.*, **34**, 742–750, doi:10.1002/joc.3718.

Zhou, T., R. Yu, H. Chen, A. Dai, and Y. Pan, 2008: Summer precipitation frequency, intensity, and diurnal cycle over China: A comparison of satellite data with rain gauge observations. *J. Climate*, **21**, 3997–4010, doi:10.1175/2008JCLI2028.1.